Cell Metabolism

Article

Itaconate and itaconate derivatives target JAK1 to suppress alternative activation of macrophages

Graphical abstract

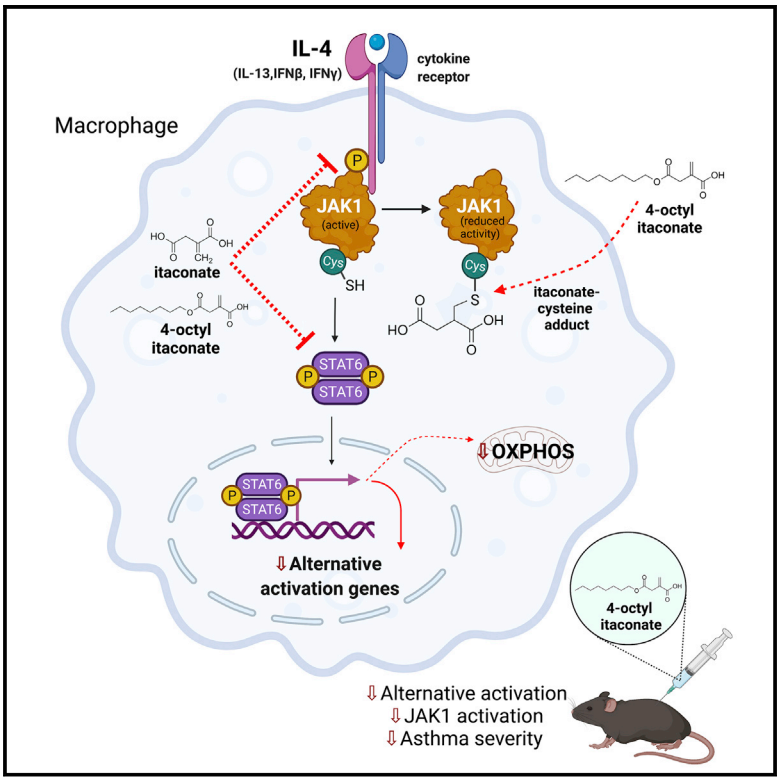

Highlights

- Itaconate reduces M2 macrophage polarization, JAK1/STAT6 activation, and OXPHOS
- Itaconate derivative OI is a JAK1 inhibitor in type 1 and 2 cytokine pathways
- Cysteine residues on JAK1 are directly modified by itaconate derivates
- Itaconate derivative OI inhibits JAK phosphorylation and asthma severity *in vivo*

Authors

Marah C. Runtsch, Stefano Angiari, Alexander Hooftman, ..., Philip M. Hansbro, Chu Wang, Luke A.J. O'Neill

Correspondence

runtschm@tcd.ie (M.C.R.), laoneill@tcd.ie (L.A.J.O.)

In brief

The wide-reaching roles of the immunomodulatory metabolite itaconate are incompletely understood. Here, Runtsch et al. demonstrate that itaconate and derivatives directly modify JAK1 and are JAK1 inhibitors during macrophage alternative activation. These discoveries provide a novel basis for itaconate and derivatives as therapies in type-2-driven diseases, including asthma.

Runtsch et al., 2022, Cell Metabolism *34*, 487–501
March 1, 2022
https://doi.org/10.1016/j.cmet.2022.02.002

CellPress

Cell Metabolism

CellPress

Article

Itaconate and itaconate derivatives target JAK1 to suppress alternative activation of macrophages

Marah C. Runtsch,[1,*] Stefano Angiari,[1,11] Alexander Hooftman,[1] Ridhima Wadhwa,[7,8] Yanling Zhang,[2] Yunan Zheng,[3] Joseph S. Spina,[4] Melanie C. Ruzek,[4] Maria A. Argiriadi,[4] Anne F. McGettrick,[1] Rui Santalla Mendez,[1] Alessia Zotta,[1] Christian G. Peace,[1] Aoife Walsh,[1] Roberta Chirillo,[5] Emily Hams,[6] Padraic G. Fallon,[6] Ranjith Jayaraman,[7] Kamal Dua,[7,8] Alexandra C. Brown,[10] Richard Y. Kim,[9,10] Jay C. Horvat,[10] Philip M. Hansbro,[7,10] Chu Wang,[2] and Luke A.J. O'Neill[1,12,*]

[1]School of Biochemistry and Immunology, Trinity Biomedical Sciences Institute, Trinity College Dublin, 152–160 Pearse Street, Dublin D02 R590, Ireland

[2]Synthetic and Functional Biomolecules Center, Beijing National Laboratory for Molecular Sciences, Key Laboratory of Bioorganic Chemistry and Molecular Engineering of Ministry of Education, Peking-Tsinghua Center for Life Sciences, Peking University, Beijing 100871, China

[3]Drug Discovery Science & Technology, AbbVie Inc., 1 North Waukegon Road, North Chicago, IL 60064, USA

[4]AbbVie, Bio Research Center, 100 Research Drive, Worcester, MA 01608, USA

[5]Department of Experimental and Clinical Medicine, "Magna Græcia" University of Catanzaro, Catanzaro, Italy

[6]School of Medicine, Trinity Biomedical Sciences Institute, Trinity College Dublin, 152–160 Pearse Street, Dublin D02 R590, Ireland

[7]Centre for Inflammation, Centenary Institute and University of Technology Sydney, Faculty of Science, School of Life Sciences, Sydney, NSW, Australia

[8]Discipline of Pharmacy, Graduate School of Health, University of Technology Sydney, Sydney, NSW, Australia

[9]School of Life Sciences, Faculty of Science, University of Technology Sydney, Sydney, NSW, Australia

[10]Priority Research Centre for Healthy Lungs, Hunter Medical Research Institute and University of Newcastle, Newcastle, NSW, Australia

[11]Present address: Division of Immunology and Pathophysiology, Otto Loewi Research Center, Medical University of Graz, Graz, Austria

[12]Lead contact

*Correspondence: runtschm@tcd.ie (M.C.R.), laoneill@tcd.ie (L.A.J.O.)

https://doi.org/10.1016/j.cmet.2022.02.002

SUMMARY

The Krebs cycle-derived metabolite itaconate and its derivatives suppress the inflammatory response in pro-inflammatory "M1" macrophages. However, alternatively activated "M2" macrophages can take up itaconate. We therefore examined the effect of itaconate and 4-octyl itaconate (OI) on M2 macrophage activation. We demonstrate that itaconate and OI inhibit M2 polarization and metabolic remodeling. Examination of IL-4 signaling revealed inhibition of JAK1 and STAT6 phosphorylation by both itaconate and OI. JAK1 activation was also inhibited by OI in response to IL-13, interferon-β, and interferon-γ in macrophages and in T helper 2 (Th2) cells. Importantly, JAK1 was directly modified by itaconate derivatives at multiple residues, including cysteines 715, 816, 943, and 1130. Itaconate and OI also inhibited JAK1 kinase activity. Finally, OI treatment suppressed M2 macrophage polarization and JAK1 phosphorylation *in vivo*. We therefore identify itaconate and OI as JAK1 inhibitors, suggesting a new strategy to inhibit JAK1 in M2 macrophage-driven diseases.

INTRODUCTION

Itaconate has recently emerged as an important regulator of immunity and inflammation, with studies highlighting its immunomodulatory effects in multiple contexts (Hooftman and O'Neill, 2019). It is one of the most highly upregulated metabolites during pro-inflammatory (M1) activation of macrophages (Hooftman and O'Neill, 2019; Lampropoulou et al., 2016; Mills et al., 2018; O'Neill and Artyomov, 2019; Weiss et al., 2018). M1 macrophages activated by lipopolysaccharide (LPS), viral components, or interferon gamma (IFN-γ) express high levels of the gene *Irg1*, also known as *Acod1*, which encodes the enzyme aconitate decarboxylase (CAD) (Hooftman and O'Neill, 2019; Lampropoulou et al., 2016; Mills et al., 2018). This enzyme uses the Krebs cycle intermediate *cis*-aconitate as a substrate and converts it into itaconate, and in this way, itaconate accumulates intracellularly and extracellularly (Lampropoulou et al., 2016). In macrophages, itaconate and itaconate derivatives have been shown to inhibit the Krebs cycle enzyme succinate dehydrogenase (SDH) and thereby block reactive oxygen species (ROS) production from complex I, leading to inhibition of hypoxia-inducible factor (HIF)-1α activity and interleukin (IL)-1β production (Lampropoulou et al., 2016; Mills et al., 2018). Itaconate and derivative compounds have also been reported to activate nuclear factor erythroid 2-related factor 2 (NRF2), leading to a boost in the antioxidant response, and to drive activating transcription factor 3 (ATF3) expression, which limits production of cytokines such as IL-6 (Bambouskova et al., 2018; Mills et al.,

2018). Additionally, itaconate has recently been shown to inhibit the NLR family pyrin domain containing 3 (NLRP3) inflammasome (Hooftman et al., 2020). Overall, evidence so far indicates that itaconate is an immunomodulatory metabolite whose targets are still being uncovered.

Itaconate and its derivatives are potent cysteine modifiers, due to its nature as an α,β-unsaturated dicarboxylic acid (Hooftman and O'Neill, 2019; Hooftman et al., 2020; Mills et al., 2018; Qin et al., 2019, 2020). This is similar to fumarate and its derivative dimethyl fumarate (DMF), which also modify cysteines, with DMF being an approved treatment for multiple sclerosis and psoriasis (Blewett et al., 2016). Itaconate and derivatives are electrophilic, and can react with thiol groups with varying electrophilicity (Bambouskova et al., 2018; Li et al., 2020). This is an alkylation reaction and is termed 2,3-dicarboxypropylation or itaconation (Hooftman and O'Neill, 2019; Mills et al., 2018; Qin et al., 2020; Zhang et al., 2021). Many studies of itaconate involve the use of the derivative compound 4-octyl itaconate (OI) because OI has enhanced cell permeability compared with itaconic acid itself, similar thiol reactivity to itaconate versus other derivatives, and is converted into itaconate intracellularly (Hooftman and O'Neill, 2019; Hooftman et al., 2020; Li et al., 2020). This compound and similar itaconate derivatives show therapeutic promise in a number of inflammatory and infectious disease models, including pulmonary fibrosis, multiple sclerosis, sepsis, SARS-CoV-2 infection, and cardiovascular disease (Hooftman and O'Neill, 2019; Jaiswal et al., 2021; Kuo et al., 2020; Mills et al., 2018; Ogger et al., 2020; Olagnier et al., 2020; Yang et al., 2020). These investigations have highlighted the potential utility of itaconic acid, OI, or similar derivatives as potential therapies for the treatment of inflammatory diseases.

While many studies have explored the roles of itaconate and derivatives in pro-inflammatory, M1 macrophages, little is known about the effects this metabolite has in other macrophage subtypes. Macrophage polarization is a diverse and complex spectrum, with many macrophages switching or adopting mixed phenotypes depending on the cytokine milieu and environmental cues (Italiani and Boraschi, 2014; Martinez and Gordon, 2014; Sica and Mantovani, 2012). In general, so-called M1 polarization gives rise to pro-inflammatory responses via enhanced glycolysis, while M2, or alternatively activated, macrophages undergo enhanced oxidative phosphorylation (OXPHOS). M2 macrophages (specifically M2a) are activated by the cytokines IL-4 and IL-13, which signal through the Janus kinase 1 (JAK1) and Signal transducer and activator of transcription 6 (STAT6) pathway. M2 macrophages express signature genes such as peroxisome proliferator-activated receptor γ (*Pparg*), mannose receptor (*Mrc1*/CD206), arginase (*Arg1*), galactose-binding lectin (*Clec10a*/CD301), and resistin-like alpha (*Retnla*/*Fizz1*), which promote wound healing and tissue remodeling (Langston et al., 2017; Viola et al., 2019). Metabolically, alternatively activated macrophages utilize glucose, glutamine, and fatty acids as fuel sources to feed OXPHOS, which is required for their polarization and function (Langston et al., 2017; Viola et al., 2019; Wang et al., 2018). While the current paradigm of M2 macrophages is that they are more anti-inflammatory, they also play a role in promoting certain immunologic diseases. For example, type 2 inflammatory responses characteristic of M2 macrophages and T helper 2 (Th2) cells are found in lung pathologies such as asthma, allergy, and fibrosis (Chávez-Galán et al., 2015).

Recently, Nelson and colleagues found that loss of PPARγ resulted in enhanced IRG1 and itaconate levels, demonstrating that this important M2-promoting regulator is acting as a brake on itaconate, which might therefore be an M2 macrophage inhibitor (Nelson et al., 2018; O'Neill and Artyomov, 2019). In addition, the M2-promoting microRNA miR-93 targets IRF9, which in turn represses IRG1 and itaconate levels during macrophage alternative activation (Ganta et al., 2017; O'Neill and Artyomov, 2019). Both of these studies show that M2 macrophages have mechanisms in place to repress IRG1, suggesting that itaconate may limit alternative activation and must be attenuated for M2 polarization. Intriguingly, M2 macrophages have also been shown to take up itaconate (Puchalska et al., 2018). We therefore assessed the impact of itaconate on alternatively activated M2 macrophages, to understand how their polarization might be affected in the presence of this metabolite. Our results indicate that itaconate and its derivative OI block M2 polarization via inhibition of the JAK1/STAT6 signaling pathway downstream of IL-4. By directly targeting JAK1, itaconate and OI are thus identified as JAK1 inhibitors, which could ultimately have utility in the treatment of type 2 immune-mediated diseases, such as allergy, asthma, and fibrosis.

RESULTS

Itaconate derivative 4-octyl itaconate blocks M2 polarization

We first investigated the effect of OI on IL-4-activated "M2" murine bone-marrow-derived macrophages (BMDMs). OI reduced the IL-4-induced expression of the M2-signature genes *Arg1*, *Fizz1*, *Mrc1*, and *Pparg* in a dose-dependent manner in BMDMs (Figures 1A–1D). There was also a significant reduction in both the percentage and mean fluorescence intensity (MFI) of the M2 surface markers CD206 (mannose receptor) (Figures 1E and 1F) and CD301 (C-type lectin domain family 10 member A) (Figures 1G and 1H) with OI treatment, compared with control.

One of the key "master" transcription factors activated in M2 macrophages is STAT6, which is required for the alternative activation program. We also observed a decrease in phosphorylated STAT6 in BMDMs treated with OI and IL-4 compared with those treated with IL-4 alone for 24 h (Figure 1I, lane 3 versus 4, and Figure 1J). OI repressed STAT6 phosphorylation at early time points up to 30 min post-IL-4 stimulation (Figure S1A, lanes 2 versus 3, 4 versus 5, and 6 versus 7). Upstream of STAT6 activation, and immediately downstream of IL-4 receptor stimulation, the tyrosine kinase JAK1 is phosphorylated, which is also required for M2 macrophage activation (Byles et al., 2013; Chawla, 2010). OI blocked phosphorylation of JAK1 after 1 h of IL-4 treatment (Figure 1K, lane 3 versus 4, and Figure 1L), and also at earlier times (5 and 10 min after IL-4 stimulation) (Figure S1B, lane 3 versus 4, 5 versus 6), indicating that OI-mediated inhibition of the M2 program happens early in the IL-4/JAK1/STAT6 signaling cascade. Reduction of phospho-JAK1 levels by OI was maintained at time points up to 24 h (data not shown). We next examined signaling further upstream, measuring expression of the cytokine receptor subunit IL-4 receptor alpha (IL4RA), which IL-4 signals through to activate JAK1 and

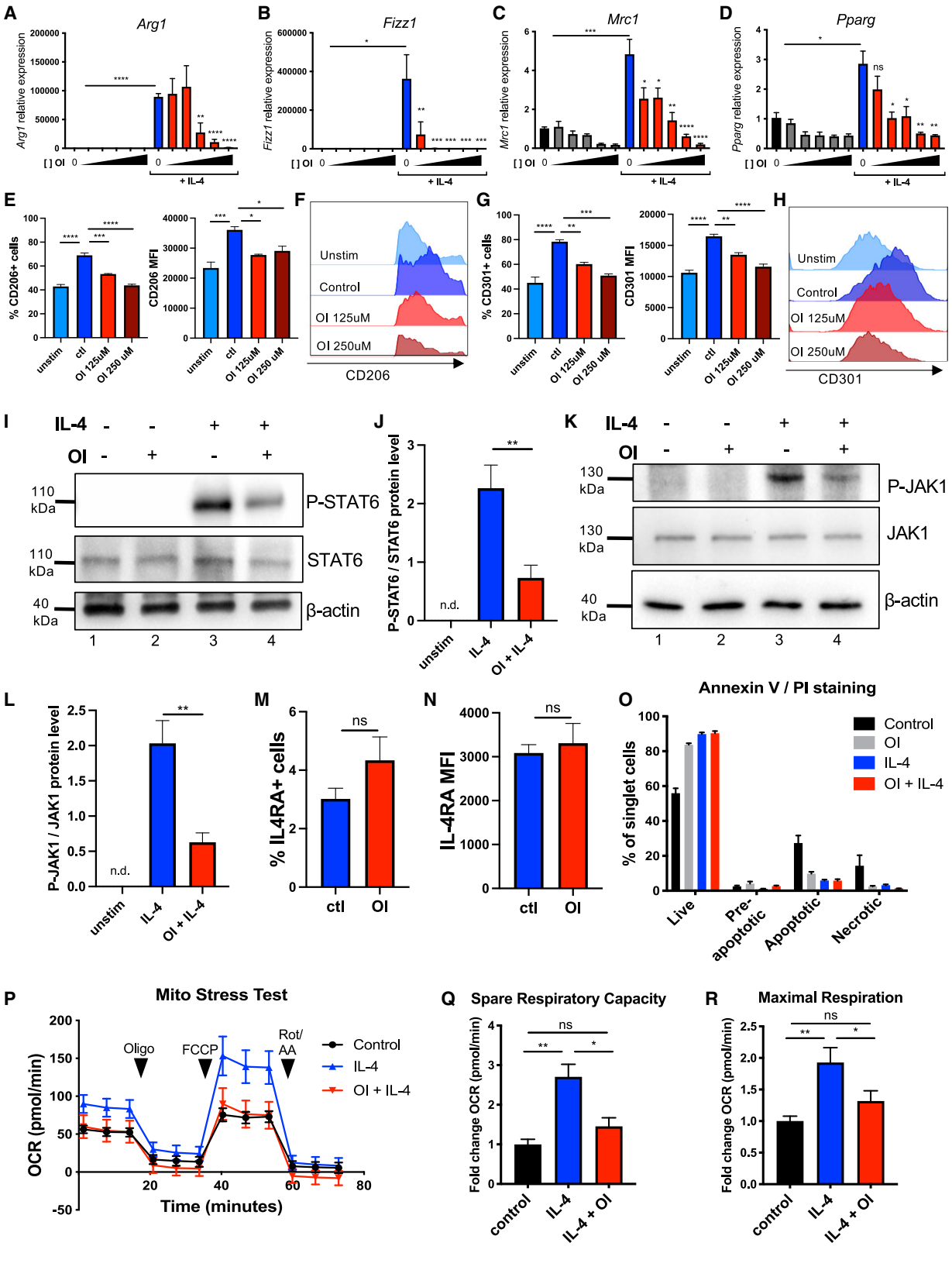

(legend on next page)

STAT6. Flow cytometric analysis of IL4RA surface expression on IL-4-treated BMDMs showed no change in the percentage or per-cell basis expression of this protein, comparing OI-treated cells to control (Figures 1M and 1N). These data suggest that OI inhibits M2 macrophage activation by blocking JAK1 phosphorylation.

OI treatment also inhibited Suppressor of cytokine signaling 1 (Socs1), another M2 marker in the JAK1/STAT6 signaling pathway (Langston et al., 2017; Viola et al., 2019) (Figure S1C, lane 2 versus 3), further indicating inhibition of IL-4 signaling. Because our results show inhibition of many of the key components of the M2 macrophage program, we measured cell death during IL-4 and OI treatment to test if the inhibitory effects of OI were due to toxicity. Annexin V and propidium iodide (PI) staining showed that OI does not induce apoptosis or necrosis in unstimulated and IL-4-activated macrophages (Figures 1O and S1G). Taken together, these data indicate an inhibitory effect of OI on early events in IL-4 signaling.

Since OI is known to activate Nrf2 (Mills et al., 2018), we measured activation of this transcription factor as a positive control to ensure efficacy of OI in this model. Our results show that treatment with OI resulted in the induction of Nrf2 protein in both M0 and M2 BMDMs (Figure S1D, lane 3 and 4). Nrf2 downstream target genes *Gclm*, *Nqo1*, and *Hmox1* also had enhanced expression upon addition of increasing doses of OI in both control and IL-4-stimulated BMDMs (Figure S1E). These results confirm that OI is not repressing gene expression globally in M2 macrophages. However, to examine OI's dependency on Nrf2 in this context, OI was tested in Nrf2-null (*Nfe2l2*$^{-/-}$) M2 macrophages. OI significantly inhibited expression of *Arg1*, *Fizz1*, and *Pparg* upon IL-4 stimulation in *Nfe2l2*$^{-/-}$ BMDMs, similar to wild-type (WT) macrophages (Figure S1F). These results demonstrate that Nrf2 is not required for the inhibitory effect of OI on M2 macrophage activation.

Next, we examined the effect of OI on metabolic reprogramming in M2 macrophages, which require OXPHOS for their polarization (Langston et al., 2017; Viola et al., 2019). Consistent with previous studies, treatment of BMDMs with IL-4 increased OXPHOS, as measured by oxygen consumption rate (OCR), compared with unstimulated macrophages (Figure 1P). Importantly, this response was inhibited in OI-treated M2 macrophages (Figure 1P). OI treatment also reduced spare respiratory capacity and maximal respiration levels in response to IL-4 compared with control (Figures 1Q and 1R). OI had no significant effect on glycolysis in IL-4-treated BMDMs (Figure S2A), nor on basal OXPHOS and glycolysis in unpolarized, control macrophages (Figures S2B and S2C).

Because OXPHOS was inhibited by OI in M2 macrophages, we tested if supplementation of the TCA cycle with alpha-ketoglutarate (αKG) could rescue OI's inhibitory effects on M2 gene expression. M2 macrophages utilize glutamine as a fuel source (Jha et al., 2015; Wang et al., 2018), which during glutaminolysis is metabolized into αKG and supplements the TCA cycle, and this process is important for the M2 metabolic program and function (Liu et al., 2017). Itaconate has previously been shown to alter glutamine metabolism in other cell types (Cordes et al., 2020). To test if OI was blocking M2 activation by affecting glutamine metabolism or the TCA cycle directly, IL-4-activated BMDMs were treated with a cell-permeable version of αKG, DM-αKG, to directly supplement the TCA cycle (Liu et al., 2017). As these cells were not glutamine starved, there were no changes in expression of the M2 genes *Arg1*, *Fizz1*, and

Figure 1. Itaconate derivative OI blocks M2 polarization

(A–D) BMDMs were pretreated with DMSO (vehicle control) or increasing concentrations of OI for 2 h, then stimulated with media or IL-4 (20 ng/mL) for 24 h. The black triangle represents increasing OI concentrations ([ ] OI) starting from the left: 31.25, 62.5, 125, 250, and 500 μM. qRT-PCR results showing mRNA expression of *Arg1* (A), *Fizz1* (B), *Mrc1* (C), and *Pparg* (D) normalized to *18s*. n = 6, 2 experimental repeats.

(E) BMDMs were pretreated with DMSO (unstim, ctl) or 125 or 250 μM OI for 2 h, then stimulated with media (unstim) or IL-4 (ctl, OI 125 μM, 250 μM) for 24 h. Flow cytometry data for the M2 surface marker CD206 (mannose receptor), showing percentage of CD206$^+$ BMDMs (left) and mean fluorescence intensity (MFI) of CD206 (right) (n = 6, showing one representative experiment of 2 repeats).

(F) Flow cytometry histograms of one representative mouse from (E); CD206 fluorescence expression in BMDMs treated with the indicated label.

(G) BMDMs were treated as in (E). Flow cytometry data for the M2 surface marker CD301 (CLEC10a), showing percentage of CD301$^+$ BMDMs (left) and mean fluorescence intensity (MFI) of CD301 (right) (n = 6, showing one representative experiment of 2 repeats).

(H) Flow cytometry histograms of one representative mouse from (G); CD301 fluorescence expression in BMDMs treated with the indicated label.

(I) WT BMDMs were pretreated with OI for 2 h, then stimulated with IL-4 for 24 h. Western blot performed on cell lysates for phosphorylated STAT6 (Tyr641), total STAT6, and β-actin housekeeping control. Showing one representative blot of n = 5.

(J) Western blot densitometry values of phosphorylated STAT6 (Tyr641) normalized to total STAT6 protein in BMDMs treated with the indicated label (n = 5).

(K) WT BMDMs were pretreated with OI for 2 h, then stimulated with IL-4 for 1 h. Western blot performed on cell lysates for phosphorylated JAK1 (Tyr1034/1035), total JAK1, and β-actin housekeeping control. Showing one representative blot of n = 5.

(L) Western blot densitometry values of phosphorylated JAK1 (Tyr1034/1035) normalized to total JAK1 protein in BMDMs treated with the indicated label (n = 5).

(M) WT BMDMs were pretreated with OI for 2 h, then stimulated with IL-4 for 24 h. Flow cytometry was performed on cells treated with IL-4 alone (ctl) or OI + IL-4, stained for the surface marker IL-4Rα (CD124). Data show percentage of IL-4Rα$^+$ BMDMs.

(N) Mean fluorescence intensity (MFI) of IL-4Rα on BMDMs (n = 6, 2 experimental repeats).

(O) WT BMDMs were pretreated with OI for 2 h, then stimulated with IL-4 for 24 h, and flow cytometry was performed on cells stained for annexin V surface expression and the DNA dye propidium iodide (PI). Percentage of singlet cells that are live (Annexin V$^-$ PI$^-$), pre- or early apoptotic (Annexin V$^+$ PI$^-$), apoptotic (Annexin V$^+$ PI$^+$), and necrotic (Annexin V$^-$ PI$^+$) (n = 3). Representative flow plots can be found in Figure S1G.

(P) WT BMDMs were pretreated with OI for 2 h, then stimulated with IL-4 for 24 h. Seahorse Mito Stress Test showing oxygen consumption rate (OCR) of cells over time after addition of oligomycin (oligo), carbonyl cyanide-4-phenylhydrazone (FCCP), and rotenone/antimycin A (Rot/AA), in unstimulated cells (control), IL-4 alone, or OI + IL-4 (n = 8, 3 experimental repeats).

(Q) Spare respiratory capacity of BMDMs that were unstimulated (control), treated with IL-4 alone, or OI + IL-4, as measured by Seahorse Mito Stress test.

(R) Maximal respiration of BMDMs that were unstimulated (control), treated with IL-4 alone, or OI + IL-4, as measured by Seahorse Mito Stress test.

Data are displayed as mean ± SEM. Differences were considered statistically significant at *p ≤ 0.05. **p ≤ 0.01, ***p ≤ 0.001, and ****p < 0.0001. See also Figures S1 and S2.

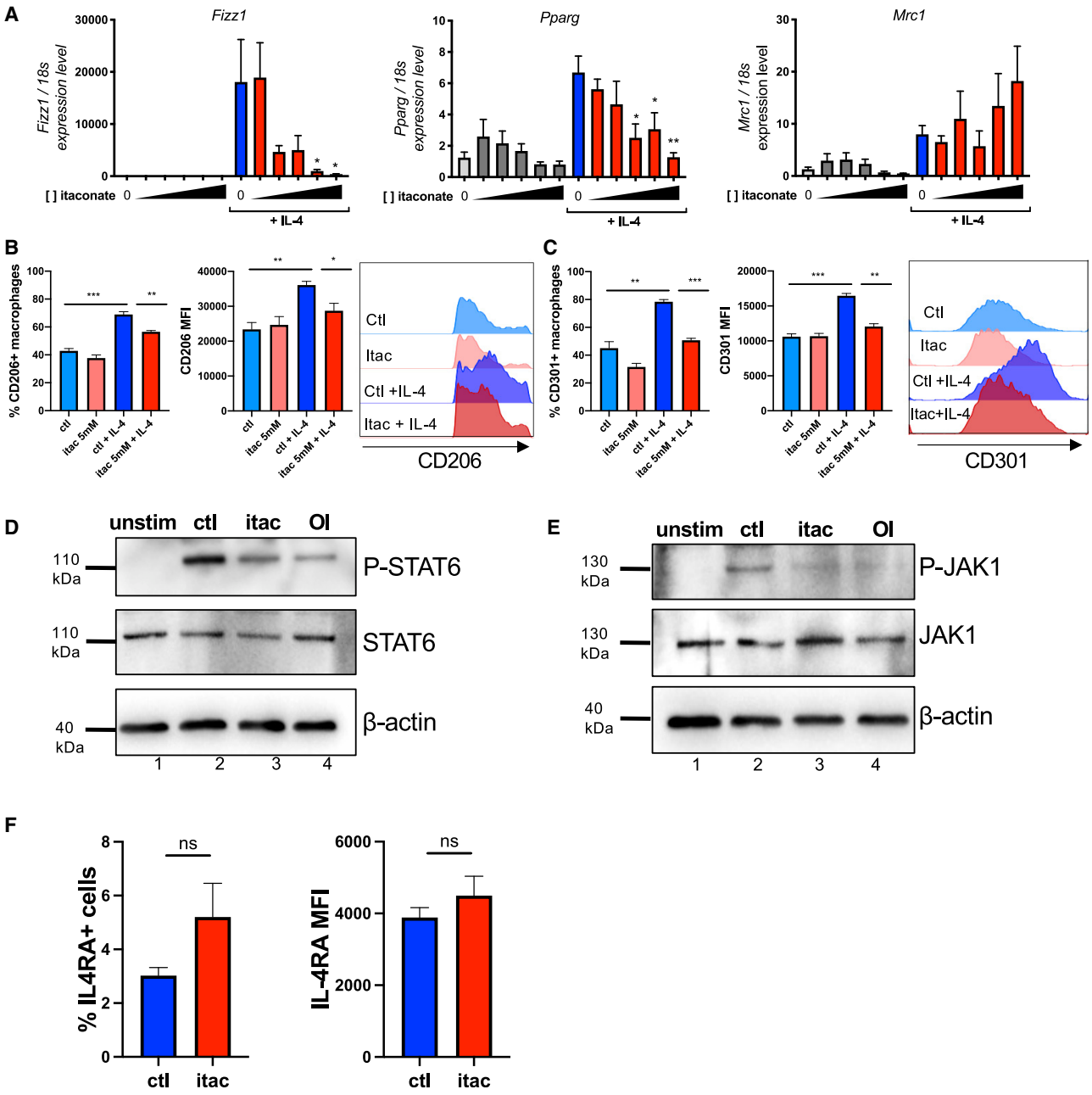

Figure 2. Itaconate blocks M2 polarization similarly to OI

(A) BMDMs were pretreated with media (0 mM itaconate) or increasing concentrations of itaconate for 2 h, then stimulated with media (ctl) or IL-4 for 24 h. The triangle represents increasing itaconate concentrations ([ ]) starting from the left: 0.31, 0.63, 1.25, 2.5, and 5 mM. qRT-PCR results showing mRNA expression of M2 genes *Fizz1*, *Pparg*, and *Mrc1*, all normalized to *18s* (n = 6, 2 experimental repeats).

(B and C) BMDMs were pretreated with media (ctl) or 5-mM itaconate for 2 h, then stimulated with media or IL-4 for 24 h. ; (B) Flow cytometry data for the M2 surface marker CD206 showing percentage of $CD206^+$ BMDMs (left) and mean fluorescence intensity (MFI) of CD206 (middle) (n = 6, showing one representative experiment of 2 repeats). Right: flow cytometry histograms of one representative mouse; CD206 fluorescence expression in BMDMs treated with the indicated label.

(C) Flow cytometry data for the M2 surface marker CD301 showing percentage of $CD301^+$ BMDMs (left) and mean fluorescence intensity of CD301 (middle) (n = 6, showing one representative experiment of 2 repeats). Right: flow cytometry histograms of one representative mouse; CD301 fluorescence expression in BMDMs treated with the indicated label.

(D and E) WT BMDMs were pretreated with itaconate (itac) or OI for 2 h, then stimulated with IL-4 for 24 h.

(D) Western blot performed on cell lysates for phosphorylated STAT6 (Tyr641), total STAT6, and β-actin housekeeping control. Showing one representative blot of n = 3.

(legend continued on next page)

Mrc1 comparing DM-αKG plus IL-4-treated cells with IL-4 treatment alone (Figure S2D). Notably, the addition of DM-αKG did not rescue the suppression of these M2 genes observed during OI treatment (Figure S2D), suggesting that the inhibitory effects of this itaconate derivative are not mediated through direct TCA cycle inhibition or altered glutamine metabolism. These data altogether demonstrate that OI inhibits IL-4-induced M2 gene expression, JAK1/STAT6 signaling, and metabolic reprogramming, with inhibition likely to be occurring at the level of JAK1 phosphorylation.

Itaconate blocks M2 polarization

We then tested whether underivatized itaconic acid could recapitulate the inhibitory effects of OI in macrophage alternative activation. Treatment of BMDMs with increasing concentrations of itaconate at a physiologic pH (~7.4, to rule out any pH-dependent effects) resulted in a decrease in IL-4-induced *Fizz1* and *Pparg* expression, while *Mrc1* (mannose receptor) mRNA expression was not significantly affected (Figure 2A). Despite mannose receptor mRNA being unaffected, surface protein expression of the mannose receptor, or CD206, was decreased in itaconate-treated M2 macrophages (Figure 2B). Itaconate treatment also decreased the percentage of $CD301^+$ cells and CD301 MFI, compared with control M2 macrophages (Figure 2C). Similar to OI, itaconate inhibited IL-4-induced STAT6 phosphorylation (Figure 2D, lane 2 versus 3 and 4). Further, phosphorylation of JAK1 was inhibited by itaconate as well as OI upon IL-4 simulation (Figure 2E, lane 2 versus 3 and 4), while IL4RA surface protein expression was not affected (Figure 2F). These data altogether indicate that itaconic acid itself can inhibit M2 macrophage polarization in a similar manner to OI.

OI suppresses activation of JAK1 in macrophages and Th2 cells

To further probe the mechanism by which OI inhibits the M2 macrophage program, we examined JAK1 activation in more detail, as it was the earliest upstream component inhibited by OI during IL-4 activation. IL-13 uses a similar cytokine signaling pathway to IL-4, including activation of JAK1 through IL4RA and IL13RA heterodimers (Jiang et al., 2000; Junttila, 2018). OI inhibited the IL-13-induced expression of M2-signature genes *Arg1*, *Mrc1*, and *Pparg* (Figure 3A). Underivatized itaconate also repressed induction of *Mrc1* and *Pparg* upon IL-13 stimulation, but not *Arg1* (Figure 3A). Importantly, OI treatment reduced JAK1 phosphorylation during IL-13 stimulation (Figures 3B and 3C), consistent with our earlier results with IL-4. Thus, OI suppresses M2 macrophage effector genes and JAK1 phosphorylation, both through IL-4 and IL-13 stimulation.

JAK1 is activated by multiple other cytokine receptors, including the interferon-α/β receptor (IFNAR). The effect of OI on JAK1 activation was therefore tested in type-I interferon (IFN)-stimulated macrophages. OI treatment resulted in a decrease of phosphorylated JAK1 levels in BMDMs stimulated with the cytokine IFN-β (Figures 3D and 3E). IFNAR stimulation by IFN-β activates STAT1 downstream of JAK1, and we found a decrease in STAT1 phosphorylation upon OI treatment compared with control IFN-β-stimulated cells (Figures 3F and 3G). Phosphorylated JAK1 was also reduced in BMDMs stimulated with interferon gamma (IFN-γ), another cytokine that utilizes JAK1 for signaling during M1 polarization (Figures S3B and S3C). These data provide further evidence for inhibition of JAK1 activation by OI upon cytokine signaling and suggest that OI inhibits JAK1 phosphorylation broadly, even outside of M2 polarization.

We also tested the effect of OI in another immune cell type that utilizes JAK1 for signaling and activation, T helper 2 subset (Th2) $CD4^+$ T cells (Ashino et al., 2014). Resting murine $CD4^+$ T cells were activated with αCD3/CD28 and stimulated with IL-4 to skew these cells to the Th2 subset. OI dose-dependently inhibited expression of the Th2 genes *Il13*, *Il5*, and *Pparg* (Figure 3H), while underivatized itaconate inhibited *Il5* and *Il13* mRNA expression (Figure S3D). JAK1 phosphorylation was also inhibited by OI in a dose-dependent manner in Th2 cells (Figure 3I, lanes 3 and 4 versus lane 2, and Figure 3J). Further, intracellular cytokine staining revealed inhibition of IL-13 production by Th2 cells upon treatment with OI (Figures 3K and 3L). Taken together, these data suggest that JAK1 is a key cellular signaling component inhibited by the itaconate derivative OI.

JAK1 is directly modified by itaconate derivatives

The inhibition of JAK1 phosphorylation in IL-4, IL-13, IFN-stimulated macrophages, and Th2 cells by OI and itaconate suggests a direct effect on the JAK1 protein. We therefore next assayed JAK1 enzymatic activity. Both itaconate and OI reduced JAK1 kinase activity by ~50% at 50 μM, demonstrating some direct inhibition on the enzyme (Figure 4A). The JAK1 inhibitors ruxolitinib, tofacitinib, and staurosporine were included as positive controls. Because itaconate and its derivatives can modify cysteine residues on many proteins and alter their function (Mills et al., 2018; Qin et al., 2019, 2020), we hypothesized that cysteines on JAK1 might be directly modified by itaconate. Suppression of JAK1 phosphorylation was maintained after OI was washed from cells prior to IL-4 treatment, suggesting a stable, covalent modification (Figures S4A and S4B).

In a recent screen, JAK1 was suggested to be modified by an itaconate bioorthogonal probe termed ITalk (Qin et al., 2020). To confirm JAK1 modification by itaconate, we overexpressed rat JAK1 in HEK293T cells, and then treated these cells with the ITalk probe. We observed an enrichment in ITalk labeling upon immunoprecipitation of JAK1, demonstrating JAK1 modification (Figure 4B). We then performed LC-MS/MS analysis and found 2,3-dicarboxypropylation of four key cysteine residues on JAK1: C715, C816, C943, and C1130 (Figures 4C and S4C). To confirm this finding in human macrophages, we profiled for

(E) Western blot performed on cell lysates for phosphorylated JAK1 (Tyr1034/1035), total JAK1, and β-actin housekeeping control. Showing one representative blot of n = 3.

(F) WT BMDMs were pretreated with 5 mM itaconate for 2 h, then stimulated with IL-4 for 24 h. Flow cytometry was performed on cells treated with IL-4 alone (ctl) or itaconate + IL-4 (itac), stained for the surface marker IL-4Rα (CD124). Left: data show percentage of $IL\text{-}4R\alpha^+$ BMDMs. Right: mean fluorescence intensity (MFI) of IL-4Rα on BMDMs (n = 6, 2 experimental repeats).
Data are displayed as mean ± SEM. Differences were considered statistically significant at $^*p \leq 0.05$. $^{**}p \leq 0.01$, $^{***}p \leq 0.001$, and $^{****}p < 0.0001$.

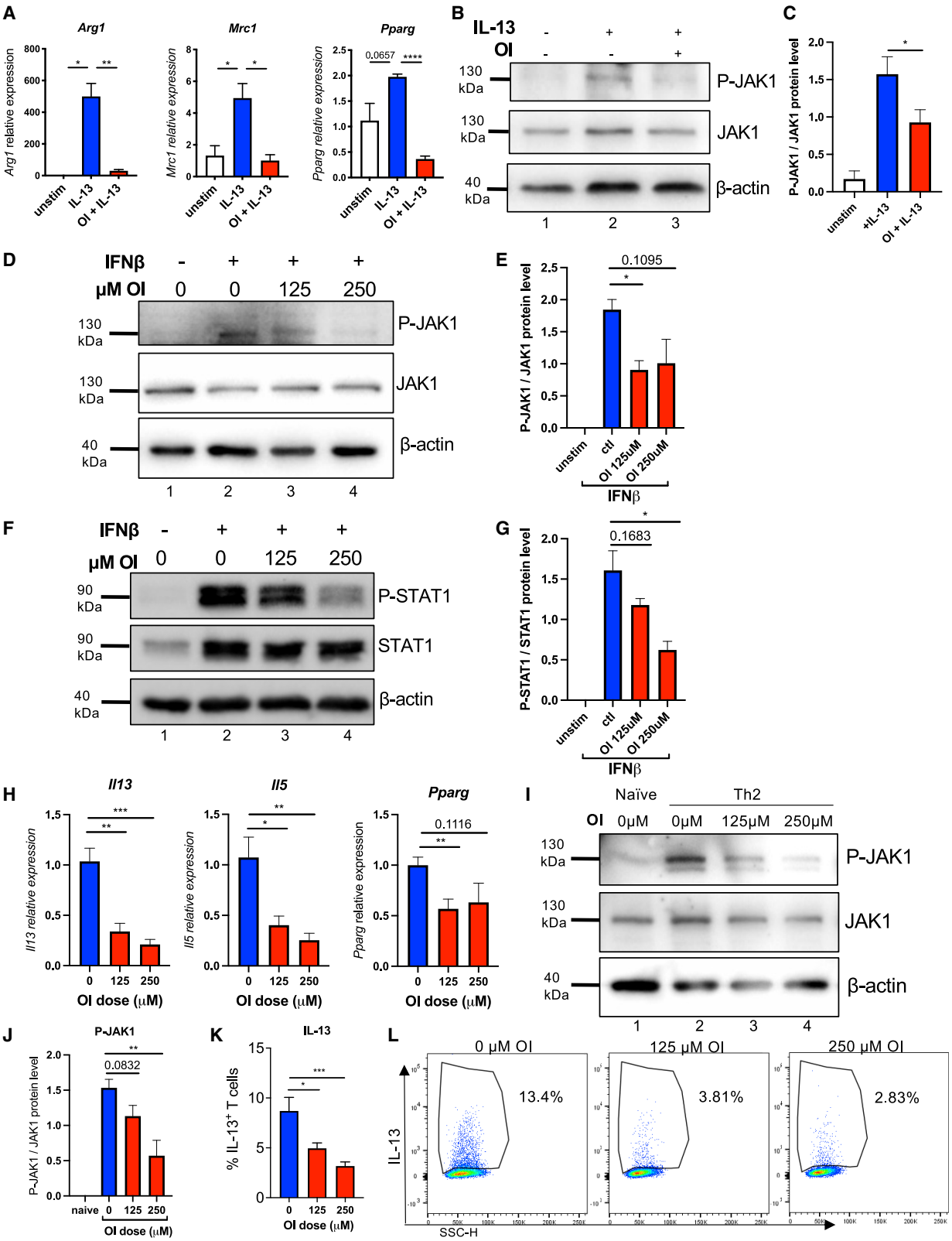

Figure 3. OI blocks JAK1 phosphorylation during IL-13, IFN-β, and Th2 stimulation

(A) BMDMs were pretreated with DMSO (unstim and IL-13) or 250 μM OI for 2 h, then stimulated with media (unstim) or IL-13 (20 ng/mL) for 24 h. qRT-PCR results showing mRNA expression of M2 genes *Arg*, *Mrc1*, and *Pparg*, all normalized to *18s* (n = 3).

(legend continued on next page)

proteins modified by OI in peripheral blood mononuclear cell (PBMC)-derived primary macrophages and found JAK1 among the top enriched proteins, with KEAP1 as a positive control (Figure S4D). Next, we performed iodoacetamide-desthiobiotin (IA-DTB)-based competitive cysteine profiling in the human macrophage cell line THP1 during OI treatment (Kuljanin et al., 2021). Among the top 10 cysteines significantly modified by OI was C817 on JAK1 (Figures 4D and 4E), corresponding to C816 on rat JAK1 observed with the ITalk probe (Figure S4E). As a positive control, C288 on KEAP1 was found to be significantly modified by OI at 125 and 250 μM (Figure 4D), which has previously been shown to be alkylated by OI (Mills et al., 2018), although KEAP1 is not required for M2 macrophage polarization (Kobayashi et al., 2016). 2,3-dicarboxypropylation of C716 and C944 were also detected, equating to the observed modification on rat C715 and C943; however, the competition ratio was not highly significant compared with control (Figure 4E). Additional OI-modified cysteines on human JAK1 were also observed but were not significant versus DMSO control (Figure 4E). Taken together, these results demonstrate that itaconate derivatives ITalk and OI directly modify C816/C817 on rodent and human JAK1, in addition to modification of C715/C716, C943/C944, and C1130/C1131 by the ITalk probe (Figures 4F and 4G). These cysteines are located within the pseudokinase and kinase domains of JAK1 (Figure 4F), which are key domains for JAK1 phosphorylation and signaling activity. These residues are highlighted within a generated 3D model of the JH1-JH2 domains of human JAK1, and additionally, showing itaconate covalently docked to C817 (Figure 4G). Amino acid sequence alignment of the four Janus kinase proteins, JAK1, JAK2, JAK3, and TYK2, revealed that a cysteine residue at amino acid 816 is unique to murine JAK1, while human TYK2 also contains a cysteine residue at the site corresponding to C817 in human JAK1 (Figure 4H). No other Janus Kinases were significantly modified by OI or ITalk in our cysteine profiling screen (data not shown) (Qin et al., 2020). Thus, JAK inhibition by OI is likely to be specific to JAK1, which is modified by this itaconate derivative at cysteine 816/817. Altogether, our data show that the inhibitory role of the itaconate derivative OI in macrophage alternative activation is likely through direct cysteine modification of JAK1 and inhibition of its kinase activity, suggesting that this itaconate derivative is a direct JAK1 inhibitor.

OI inhibits M2 macrophages and JAK1 activation *in vivo*

Finally, we tested whether OI has similar M2-inhibitory effects *in vivo*. We first utilized the IL-4-anti-IL-4 mAB complex (IL-4c) murine model, comparing mice that were injected with OI to vehicle control. As expected, treatment of mice with IL-4c resulted in enhanced expression of M2 genes in peritoneal exudate cells (PECs), as measured by mRNA expression of *Arg1*, *Fizz1*, *Ym1*, *Mrc1*, and *Pparg* (Figures 5A–5E). IL-4c-treated mice that were injected with OI showed decreased *Arg1* (Figure 5A), *Fizz1* (Figure 5B), and *Ym1* (Figure 5C) mRNA expression compared with controls, with a more minor repression of *Mrc1* (Figure 5D) and *Pparg* (Figure 5E).

IL-4c treatment also resulted in an increase in phospho-STAT6 (Figure 5G) and phospho-JAK1 (Figure 5I) in PECs. Similar to the *in vitro* results, OI treatment decreased phosphorylated STAT6 during IL-4c treatment (Figures 5F and 5G). Importantly, phospho-JAK1 levels were reduced in PECs from mice treated with OI (Figures 5H and 5I).

Next, we performed a previously established murine model of severe steroid-resistant asthma using ovalbumin (Ova) and *Chlamydia muridarum* (Cmu), a natural mouse respiratory pathogen (Horvat et al., 2007; Kim et al., 2017b; Wadhwa et al., 2019). Mice treated with Ova and Cmu develop airway inflammation, infiltration of immune cells, and other features that represent that of asthma and allergic airway diseases, and they do not respond to steroid treatment with dexamethasone (DEX) (Wadhwa et al., 2019). As expected, WT mice treated with Ova/Cmu had enhanced airway resistance (Rn) compared with sham-treated, control animals (Figures 5J and 5K). Treatment with DEX did not improve Rn, but importantly, OI significantly reduced Rn in Ova/Cmu-treated mice (Figures 5J and 5K). Ova/Cmu-treated animals and those also given Ova/Cmu plus DEX had increased macrophage infiltration into the

(B) Western blot performed on cell lysates for phosphorylated JAK1 (Tyr1034/1035), total JAK1, and β-actin housekeeping control after BMDMs were pretreated with DMSO or 250 μM OI for 2 h, then stimulated with IL-13 (20 ng/mL) for 1 h. Showing one representative blot of n = 7.
(C) Western blot densitometry values of phosphorylated JAK1 normalized to total JAK1 protein in BMDMs treated with the indicated label (n = 7).
(D) Western blot performed on cell lysates for phosphorylated JAK1 (Tyr1034/1035), total JAK1, and β-actin housekeeping control after BMDMs were pretreated with DMSO (0 μM) or 125 or 250 μM OI for 2 h, then stimulated with IFN-β (20 ng/mL) for 1 h.
(E) Western blot densitometry values of phosphorylated JAK1 (Tyr1034/1035) normalized to total JAK1 protein in BMDMs treated with the indicated label (n = 3, 2 experimental repeats).
(F) Western blot performed on cell lysates for phosphorylated STAT1, total STAT1, and β-actin housekeeping control after BMDMs were pretreated with DMSO (0 μM) or 125 or 250 μM OI for 2 h, then stimulated with IFN-β (20 ng/mL) for 24 h.
(G) Western blot densitometry values of phosphorylated STAT1 normalized to total STAT1 protein in BMDMs treated with the indicated label (n = 3, 2 experimental repeats).
(H) Murine splenic resting $CD4^+$ T cells were treated with DMSO (0 μM OI) or 125 or 250 μM OI and activated with αCD3/CD28 and skewed to Th2 with IL-4 and α-IFN-γ for 72 h. qRT-PCR results showing mRNA expression of *Il13*, *Il5*, and *Pparg*, all normalized to *Tbp* (n = 5, 2 experimental repeats).
(I) Resting $CD4^+$ T cells were treated with DMSO (0 μM OI) or 125 or 250 μM OI and activated and skewed to Th2 for 24 h. Western blot performed on cell lysates for phosphorylated JAK1 (Tyr1034/1035), total JAK1, and β-actin housekeeping control. Showing one representative blot of n = 4.
(J) Western blot densitometry values of phosphorylated JAK1 (Tyr1034/1035) normalized to total JAK1 protein in BMDMs treated with the indicated label (n = 4, 3 experimental repeats).
(K) Resting $CD4^+$ T cells were treated with DMSO (0 μM OI) or 125 or 250 μM OI and activated and skewed to Th2 for 72 h. Intracellular staining of IL-13, measured by flow cytometry, showing percentage of cells producing IL-13 (n = 6, 2 experimental repeats).
(L) Representative flow plot from one mouse showing IL-13 expression in $CD4^+$ Th2 cells treated with the indicated concentration of OI.
Data are displayed as mean ± SEM. Differences were considered statistically significant at *p ≤ 0.05. **p ≤ 0.01, ***p ≤ 0.001, and ****p < 0.0001. See also Figures S2 and S3.

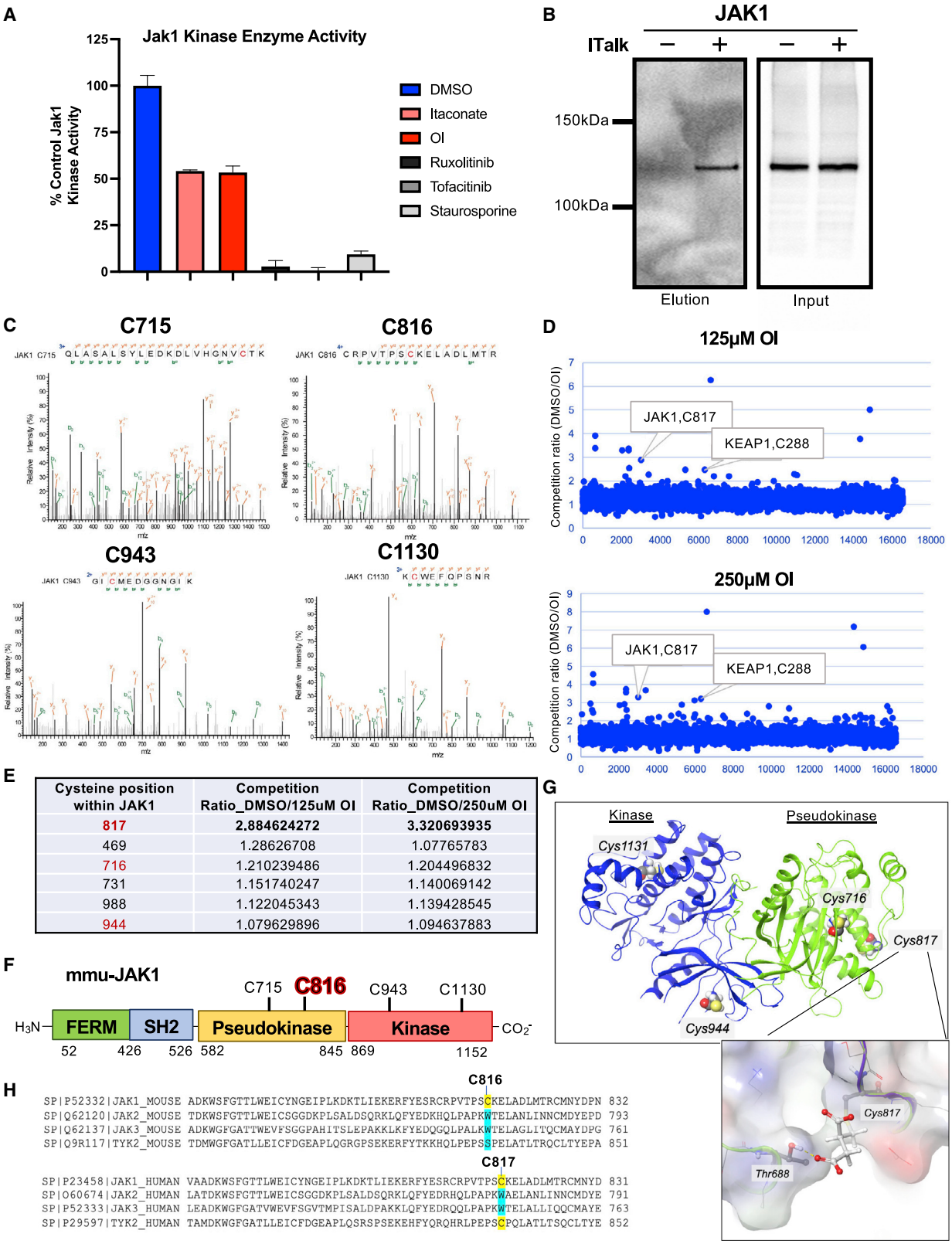

Cysteine position within JAK1	Competition Ratio_DMSO/125uM OI	Competition Ratio_DMSO/250uM OI
817	**2.884624272**	**3.320693935**
469	1.28626708	1.07765783
716	1.210239486	1.204496832
731	1.151740247	1.140069142
988	1.122045343	1.139428545
944	1.079629896	1.094637883

Figure 4. JAK1 is directly modified by itaconate derivatives

(A) JAK1 kinase activity was measured after pre-incubating recombinant JAK1 for 1 h with 50 μM DMSO (control), itaconate, OI, ruxolitinib, tofacitinib, or staurosporine. Data show kinase activity as percent relative to DMSO control.

(legend continued on next page)

bronchoalveolar lavage fluid (BALF), while OI-treated mice showed significantly reduced macrophage levels in the BALF (Figure 5L). Furthermore, mRNA expression of M2-signature genes was increased in the lungs of Ova/Cmu and Ova/Cmu/DEX-treated groups, while OI repressed *Arg1*, *Fizz1*, *Ym1*, and *Mrc1* expression (Figures 5M–5P). Finally, OI-treated mice had decreased JAK1 activation in lung tissue, compared with Ova/Cmu and Ova/Cmu/DEX. Notably, JAK1 phosphorylation levels were reduced in the lung tissue from OI-treated mice compared with Ova/Cmu alone (Figures 5Q and 5R). These results confirm our *in vitro* findings and show that OI inhibits the IL-4 signaling pathway, M2 polarization, and JAK1 activation in two different *in vivo* models. Taken together, our data point to itaconate and OI as inhibitors of JAK1 *in vitro* and *in vivo*.

DISCUSSION

Our data demonstrate that itaconate and OI inhibit phosphorylation of JAK1, identifying another mechanism for the immunomodulatory effects of itaconate. JAK inhibitors, or "jakinibs," are effective therapies in a multitude of inflammatory diseases, including rheumatoid arthritis, inflammatory bowel disease, psoriasis, and atopic dermatitis (Schwartz et al., 2017). JAKs have been shown to be sensitive to redox regulation and cysteine modification, in which the cellular redox state affects the activation of JAK proteins and thus the immunologic status of the cell (Duhé, 2013; Smith et al., 2012). JAK3 has also been shown to be covalently modified by some jakinibs, including ritlecitinib, at Cys909 (Forster et al., 2017; Goedken et al., 2015). Specific cysteine residues on JAK2 have also been found to be redox-sensitive, with these amino acids affecting the catalytic activity of the enzyme (Smith et al., 2012). Interestingly, one of these cysteines that regulates the redox-sensitive switch in JAK2, C917 (Duhé, 2013; Smith et al., 2012), aligns with the homologous residue C943 on JAK1, found to be modified by the itaconate derivative ITalk in our study. As a known cysteine modifier, itaconate could well form the basis for a new class of JAK1 inhibitors.

OI inhibited JAK1 phosphorylation in IL-4-, IL-13-, and type-I- and II-IFN-activated macrophages, as well as in Th2 cells. All of these cytokines and cell types utilize JAK1 for downstream signaling. Chemoproteomic profiling of the itaconate modification 2,3-dicarboxypropylation (or "itaconation") in macrophages found that JAK1 is modified by the itaconate derivative ITalk (Qin et al., 2020) and our data confirm this finding with OI, in both a human macrophage cell line and primary human macrophages. We observed JAK1 modification at four key cysteine residues in rat JAK1, C715, C816, C943, and C1130, and one conserved cysteine in human JAK1, C817. JAK1 kinase activity was inhibited by OI and itaconate, most likely via modification of these cysteine residues. C816/817 and C715 are located in the pseudokinase domain of JAK1, while C943 and C1130 are within the kinase domain, and with 3D modeling, we speculate that the 2,3-dicarboxypropylation of JAK1 somehow disrupts the protein's structure to reduce kinase activity (Duhé, 2013). It is also possible that the JAK1 modification by itaconate derivatives interrupts the interaction of this tyrosine kinase with the IL-4 receptor or other accessory proteins that are required for JAK1 phosphorylation.

Itaconate and its derivatives have previously been shown to have anti-inflammatory effects during M1 macrophage activation. M1 and M2 macrophages are often viewed as a "yin and yang" dichotomy of inflammatory states, with M2 alternative activation often cited as being anti-inflammatory. Our results show that itaconate represses macrophage activation in general, rather than promoting a particular polarization state. Indeed, JAK1 is a tyrosine kinase that is commonly used by many cytokine receptors, including IL-4, IL-13, IL-2, and type-I and -II interferons. Thus, itaconate's inhibition of JAK1 phosphorylation might reduce activation of any cytokine pathway that uses JAK1 for activation and polarization. The ability of OI to inhibit glycolytic activation of pro-inflammatory "M1" macrophages (Liao et al., 2019) and IL-4-stimulated "M2" macrophages (our results) suggests that any macrophage on the "M1-M2" spectrum would have reduced function in a disease setting driven by activated macrophages. Many *in vivo* and clinical disease states contain a considerable amount of heterogeneity within the "M1-M2" spectrum (Chimal-Ramírez et al., 2016; Rőszer, 2015; Sica and Mantovani,

(B) HEK293T cells were transfected with a rat JAK1-FLAG overexpression plasmid for 24 h and then treated with 100 μM ITalk or DMSO for 12 h. The samples before and after enrichment were analyzed by anti-FLAG immunoblotting.
(C) LC-MS/MS spectra of ITalk modifications on rat JAK1 following 2-h treatment with ITalk itaconate probe, showing 2,3-dicarboxypropylation of cysteines C715, C816, C943, and C1130 (n = 3).
(D) THP1 cells were pretreated with DMSO control or 125 or 250 μM OI for 16 h, before treatment with IA-DTB, cell lysis, and measurement of modified cysteines via LC-MS. Competition ratio of modified cysteines in DMSO control compared with OI treatment, with each blue dot representing a specific cysteine on a protein. JAK1 C817 and KEAP1 C288 are highlighted among the top cysteines significantly modified over control. Showing 1 representative plot of 3 independent experiments.
(E) Raw competition ratio values of detected cysteines within JAK1 showing 2,3-dicarboxypropylation with 125 or 250 μM OI treatment. C817 is shown in bold because of its high competition ratios over DMSO control, indicating significant enrichment. Cysteines in red are those that overlap with residues modified by ITalk in rat JAK1. Showing representative data of 3 independent experiments.
(F) Schematic of murine JAK1 protein, showing amino acid positions of the FERM, SH2, pseudokinase, and kinase domains, as well as positions of itaconate-modified cysteines within JAK1, with C816 (human 817) highlighted.
(G) 3D structure of JH1-JH2 (pseudokinase and kinase) domains of human JAK1 with Cys716, Cys817, Cys994, and Cys1131 highlighted in spheres (upper). Itaconate covalently docked to Cys817. Thr688 is proximal and potentially engages in a hydrogen-bond interaction with a carbonyl group from itaconate (lower).
(H) Uniprot amino acid sequence alignment of mouse JAK1, JAK2, JAK3, and TYK2, showing a cysteine residue at site 816 in JAK1, tryptophan at the homologous sites in JAK2 and JAK3, and a serine in TYK2 (top). Uniprot animo acid sequence alignment of human JAK1, JAK2, JAK3, and TYK2, showing a cysteine residue at site 817 in JAK1, tryptophan at the homologous sites in JAK2 and JAK3, and a cysteine in TYK2 (bottom).
Data are displayed as mean ± SEM. Differences were considered statistically significant at *$p \leq 0.05$. **$p \leq 0.01$, ***$p \leq 0.001$, and ****$p < 0.0001$. See also Figure S4.

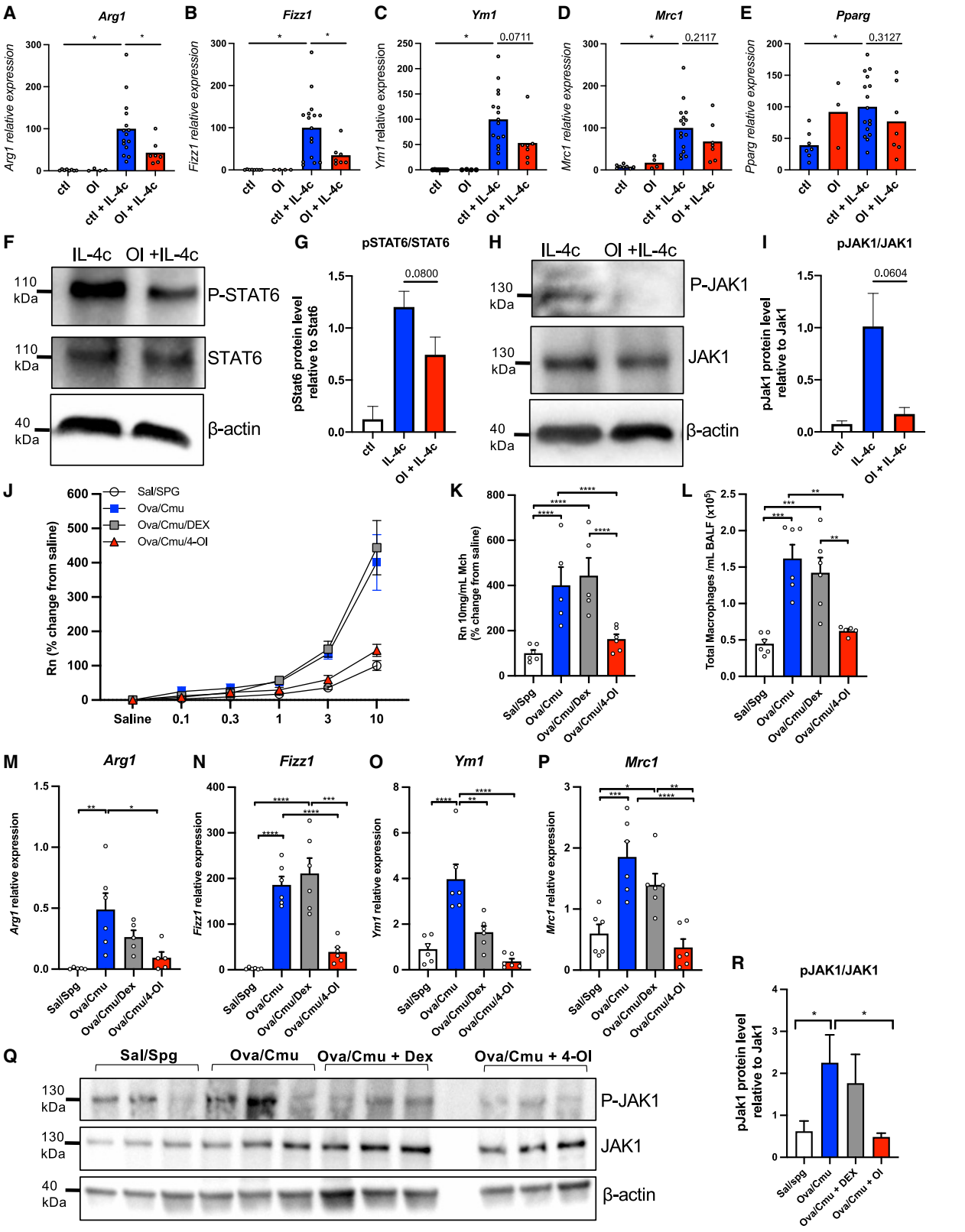

(legend on next page)

2012). Thus, we hypothesize that itaconate derivatives are an effective therapy in many disease models because of their generally inhibitory properties in macrophages. In the context of cancer, itaconate has been shown to have tumor-promoting properties (Weiss et al., 2018). Our data demonstrate that itaconate can inhibit M2 macrophages, suggesting that it might inhibit activation of tumor-associated macrophages (TAMs), which indeed have M2 properties and promote tumor growth (Mantovani et al., 2002). Thus, further work is still needed to differentiate the effect itaconate and derivatives have in TAMs and other resident and infiltrating myeloid cells, versus their direct role in tumor cells which has been previously investigated (Weiss et al., 2018).

In a recent paper by Willenborg et al., the authors demonstrate that in a model of wound healing, early-stage macrophages are glycolytic, promoting angiogenesis and inflammation. However, late-stage macrophages, activated by IL-4 and IL-13, drive OXPHOS, including the mitochondrial unfolded protein response, which in turn leads to mitohormesis and tissue repair (Willenborg et al., 2021). While this process is dependent upon cytokine signaling through IL-4Rα, whether JAK1 directly regulates mitochondrial dynamics and metabolic remodeling requires further investigation. Since itaconate attenuates IL-4 and IL-13 signaling via JAK1, this metabolite would be expected to limit OXPHOS in that context as well, potentially modulating the repair process. Thus, it may be important to attenuate itaconate production for macrophages to appropriately switch to an "M2-like" late-stage metabolic state during wound healing. The overall broader metabolic consequences of inhibiting IL-4 and IL-13 signaling in macrophages requires further investigation.

Our results are important in considering how extracellular itaconate might target M2 macrophages. Mining of publicly available data showed that IL-4-activated macrophages have STAT6- and PPARγ- dependent mechanisms in place to repress *Irg1* (Szanto et al., 2010), suggesting that itaconate is indeed inhibitory for M2 polarization. How *Irg1* is regulated in M2 macrophages requires further work. We performed experiments with OI and underivatized itaconate in parallel and observed similar effects between the two compounds on M2 macrophage activation. Some effects were less potent with itaconate than with OI, and it should be noted that experiments with itaconate were performed at higher concentrations in the mM range (similar to what is found in an LPS-stimulated macrophage) (Hooftman et al., 2020; Mills et al., 2018), while OI is immunomodulatory at concentrations in the μM range. Even so, it is clear that both compounds have a strong effect on the IL-4 cytokine signaling pathway in repressing phosphorylation of JAK1 and STAT6. We have recently confirmed that OI is effectively converted into itaconate in macrophages, even in the absence of LPS (Hooftman et al., 2020). This supports the use of the cell-permeable derivative OI to study the roles of itaconate.

While underivatized itaconate is important for understanding the physiologic relevance of this metabolite, OI also represents a pharmacological compound that mimics itaconate more potently. This is similar to the Krebs-cycle-derivative compound, DMF, which is a methyl ester of fumarate. DMF has been useful in understanding biochemical mechanisms of endogenous fumarate, while also being potently immunomodulatory and clinically approved to treat inflammatory diseases (Kornberg et al., 2018; Ryan et al., 2019). Itaconate derivatives may prove to be potent and safe pharmacological agents that might be used to treat inflammatory diseases, including those driven by alternative macrophage activation, such as asthma, allergy, and fibrosis.

Limitations of study

Our study shows that OI and itaconate repress activation of JAK1 most likely via modification of cysteine residues on JAK1. While these results show an association between the cysteine modifications and reduction in JAK1 phosphorylation, the evidence linking these two events is somewhat indirect. Further, modifications of JAK1 by endogenous itaconate could be examined in LPS-stimulated macrophages comparing WT and cells lacking *Irg1*/*Acod1*. The physiological relevance of endogenous itaconate in M2 macrophages could be further explored. M2 (IL-4) macrophages do not produce itaconate, but whether M1 macrophages or other itaconate-producing cells can communicate with M2 or similar cell types to repress their activation *in vivo* is an interesting concept that requires further study. One recent publication showed that IL-33 activated macrophages have a GATA3-dependent but IL-4-independent induction of itaconate (Faas et al., 2021), suggesting

Figure 5. OI inhibits M2 macrophages and JAK1 activation *in vivo*

(A–E) WT mice were i.p. injected with 50 mg/kg OI on days 0 and 2, followed by IL-4c i.p. injection 3 h later on days 0 and 2. Peritoneal exudate cells (PECs) were collected on day 4. qRT-PCR results showing mRNA expression of *Arg1* (A), *Fizz1* (B), *Ym1* (C), *Mrc1* (D), and *Pparg* (E) normalized to *18s*. n = 8 (ctl), 8 (OI), 16 (ctl + IL-4c), and 7 (OI + IL-4c).

(F–I) WT mice were i.p. injected with 50 mg/kg OI, followed by IL-4c i.p. injection 3 h later. PECs were collected after 5 h IL-4c treatment.

(F) Representative western blot performed on cell lysates for phosphorylated STAT6, STAT6, and β-actin housekeeping control.

(G) Densitometry values of pSTAT6 western blot bands normalized to total STAT6 (n = 6).

(H) Western blot performed on cell lysates for phosphorylated JAK1, JAK1, and β-actin housekeeping control.

(I) Densitometry values of pJAK1 western blot bands normalized to total JAK1 (n = 3).

(J) WT mice were treated with sham control (Sal/SPG), ovalbumin (Ova), and *Chlamydia muridarum* (Cmu) to induce severe steroid-resistant asthma, or Ova/Cmu plus dexamethasone (DEX), or Ova/Cmu plus OI. Airway hyperresponsiveness in terms of airway resistance (Rn) in response to increasing doses of methacholine (Mch) (n = 6).

(K) Airway resistance in response to 10 mg/mL Mch.

(L) Number of macrophages in bronchoalveolar lavage fluid (BALF).

(M–P) mRNA expression in lung tissue after asthma induction of (M) *Arg1*, (N) *Fizz1*, (O) *Ym1*, and (P) *Mrc1* (n = 6).

(Q) Western blot performed on lung tissue lysates for pJAK1, total JAK1, and β-actin housekeeping control following asthma induction.

(R) Western blot densitometry values of pJAK1 normalized to total JAK1 from lung tissue lysates after asthma treatment (n = 6).
Data are displayed as mean ± SEM. Differences were considered statistically significant at *p $\leq$ 0.05. **p $\leq$ 0.01, ***p $\leq$ 0.001, and ****p < 0.0001.

specificity of endogenous itaconate induction in macrophage polarization states. Thus, future work is needed to differentiate roles of itaconate endogenously versus exogenously in cell-cell communication.

STAR★METHODS

Detailed methods are provided in the online version of this paper and include the following:

- KEY RESOURCES TABLE
- RESOURCE AVAILABILITY
  - Lead contact
  - Materials availability
  - Data and code availability
- EXPERIMENTAL MODEL AND SUBJECT DETAILS
  - Mice
  - Murine bone marrow-derived macrophage (BMDM) culture
  - Macrophage activation
  - Treatment of cells with OI and itaconate
  - T Cell isolation and culture
  - *In vivo* IL-4 complex murine model
  - Experimental asthma infection murine model
- METHOD DETAILS
  - RNA extraction and qPCR
  - Western blotting
  - Flow cytometry
  - Seahorse metabolic assays
  - JAK1 kinase enzymatic activity assay
  - Validation of ITalk labeling of JAK1
  - Identification of JAK1 modification sites by ITalk
  - Data analysis of JAK1 modification by ITalk
  - Profiling of OI modification in human macrophages
  - Quantitative profiling of OI modified cysteinome
  - JAK1 structural modeling
- QUANTIFICATION AND STATISTICAL ANALYSIS

SUPPLEMENTAL INFORMATION

Supplemental information can be found online at https://doi.org/10.1016/j.cmet.2022.02.002.

ACKNOWLEDGMENTS

This project was funded by grants from the Science Foundation Ireland, Wellcome Trust, and European Research Council. We would like to thank the laboratory of Professor Richard Hartley at University of Glasgow, Scotland, for originally synthesizing and providing the compound 4-octyl itaconate to our lab. We thank Professor Albena Dinkova-Kostova and Elena Knatko at University of Dundee, Scotland, for kindly donating the Nfe2l2$^{-/-}$ and matched WT mouse bones for experiments. We would also like to thank Dr. Barry Moran at the Trinity Biosciences Medical Institute Flow Cytometry Core Facility for his help with use of the flow cytometers, and the Transgenics Core Facility at Trinity College Dublin.

AUTHOR CONTRIBUTIONS

Conceptualization, M.C. Runtsch and L.A.J.O.; methodology, M.C. Runtsch, S.A., A.H., and L.A.J.O.; validation, S.A., A.H., Y. Zhang, Y. Zheng, J.S.S., M.C. Ruzek, R.S.M., A.Z., C.G.P., A.W., and R.C.; formal analysis, M.C. Runtsch, S.A., R.W., Y. Zhang, and Y. Zheng; investigation, M.C. Runtsch, S.A., A.H., R.W., Y. Zhang, Y. Zheng, J.S.S., M.C. Ruzek, M.A.A., A.F.M., R.S.M., A.Z., C.G.P., A.W., R.C., E.H., P.G.F., R.J., R.Y.K., K.D., A.C.B., and J.C.H.; resources, Y. Zheng, J.S.S., M.C. Ruzek, M.A.A., P.G.F., P.M.H., C.W., and L.A.J.O.; writing – original draft, M.C. Runtsch and L.A.J.O.; writing – review & editing, M.C. Runtsch, S.A., A.H., M.C. Ruzek, and L.A.J.O.; visualization, M.C. Runtsch, S.A., A.H., Y. Zheng, and M.A.A.; supervision, M.C. Runtsch, M.C. Ruzek, P.G.F., P.M.H., C.W., and L.A.J.O.; funding acquisition, L.A.J.O.

DECLARATION OF INTERESTS

Y. Zheng, J.S.S., M.C. Ruzek, and M.A.A. are employees and shareholders of AbbVie. All other authors declare no competing interests related to this manuscript.

INCLUSION AND DIVERSITY

One or more of the authors of this paper self-identifies as a member of the LGBTQ+ community. While citing references scientifically relevant for this work, we also actively worked to promote gender balance in our reference list. The author list of this paper includes contributors from the location where the research was conducted who participated in the data collection, design, analysis, and/or interpretation of the work.

Received: June 23, 2021
Revised: November 24, 2021
Accepted: February 2, 2022
Published: March 1, 2022

REFERENCES

Ashino, S., Takeda, K., Li, H., Taylor, V., Joetham, A., Pine, P.R., and Gelfand, E.W. (2014). Janus kinase 1/3 signaling pathways are key initiators of TH2 differentiation and lung allergic responses. J. Allergy Clin. Immunol. *133*, 1162–1174.

Bambouskova, M., Gorvel, L., Lampropoulou, V., Sergushichev, A., Loginicheva, E., Johnson, K., Korenfeld, D., Mathyer, M.E., Kim, H., Huang, L.H., et al. (2018). Electrophilic properties of itaconate and derivatives regulate the IκBζ-ATF3 inflammatory axis. Nature *556*, 501–504.

Blewett, M.M., Xie, J., Zaro, B.W., Backus, K.M., Altman, A., Teijaro, J.R., and Cravatt, B.F. (2016). Chemical proteomic map of dimethyl fumarate-sensitive cysteines in primary human T cells. Sci. Signal *9*, rs10.

Byles, V., Covarrubias, A.J., Ben-Sahra, I., Lamming, D.W., Sabatini, D.M., Manning, B.D., and Horng, T. (2013). The TSC-mTOR pathway regulates macrophage polarization. Nat. Commun. *4*, 2834.

Chávez-Galán, L., Olleros, M.L., Vesin, D., and Garcia, I. (2015). Much more than M1 and M2 macrophages, there are also CD169+ and TCR+ macrophages. Front. Immunol. *6*, 263.

Chawla, A. (2010). Control of macrophage activation and function by PPARs. Circ. Res. *106*, 1559–1569.

Chi, H., Liu, C., Yang, H., Zeng, W.F., Wu, L., Zhou, W.J., Wang, R.M., Niu, X.N., Ding, Y.H., Zhang, Y., et al. (2018). Comprehensive identification of peptides in tandem mass spectra using an efficient open search engine. Nat. Biotechnol. *36*, 1059–1061.

Chimal-Ramírez, G.K., Espinoza-Sánchez, N.A., Chávez-Sánchez, L., Arriaga-Pizano, L., and Fuentes-Pananá, E.M. (2016). Monocyte differentiation towards protumor activity does not correlate with M1 or M2 phenotypes. J. Immunol. Res. *2016*, 6031486.

Cordes, T., Lucas, A., Divakaruni, A.S., Murphy, A.N., Cabrales, P., and Metallo, C.M. (2020). Itaconate modulates tricarboxylic acid and redox metabolism to mitigate reperfusion injury. Mol. Metab. *32*, 122–135.

Duhé, R.J. (2013). Redox regulation of Janus kinase: the elephant in the room. JAKSTAT *2*, e26141.

Essilfie, A.T., Horvat, J.C., Kim, R.Y., Mayall, J.R., Pinkerton, J.W., Beckett, E.L., Starkey, M.R., Simpson, J.L., Foster, P.S., Gibson, P.G., and Hansbro,

P.M. (2015). Macrolide therapy suppresses key features of experimental steroid-sensitive and steroid-insensitive asthma. Thorax *70*, 458–467.

Faas, M., Ipseiz, N., Ackermann, J., Culemann, S., Grüneboom, A., Schröder, F., Rothe, T., Scholtysek, C., Eberhardt, M., Böttcher, M., et al. (2021). IL-33-induced metabolic reprogramming controls the differentiation of alternatively activated macrophages and the resolution of inflammation. Immunity *54*, 2531–2546.e5.

Finkelman, F.D., Madden, K.B., Morris, S.C., Holmes, J.M., Boiani, N., Katona, I.M., and Maliszewski, C.R. (1993). Anti-cytokine antibodies as carrier proteins. Prolongation of in vivo effects of exogenous cytokines by injection of cytokine-anti-cytokine antibody complexes. J. Immunol. *151*, 1235–1244.

Forster, M., Gehringer, M., and Laufer, S.A. (2017). Recent advances in JAK3 inhibition: isoform selectivity by covalent cysteine targeting. Bioorg. Med. Chem. Lett. *27*, 4229–4237.

Ganta, V.C., Choi, M.H., Kutateladze, A., Fox, T.E., Farber, C.R., and Annex, B.H. (2017). A MicroRNA93-interferon regulatory factor-9-immunoresponsive gene-1-itaconic acid pathway modulates M2-like macrophage polarization to revascularize ischemic muscle. Circulation *135*, 2403–2425.

Goedken, E.R., Argiriadi, M.A., Banach, D.L., Fiamengo, B.A., Foley, S.E., Frank, K.E., George, J.S., Harris, C.M., Hobson, A.D., Ihle, D.C., et al. (2015). Tricyclic covalent inhibitors selectively target Jak3 through an active site thiol. J. Biol. Chem. *290*, 4573–4589.

Hooftman, A., and O'Neill, L.A.J. (2019). The immunomodulatory potential of the metabolite itaconate. Trends Immunol *40*, 687–698.

Hooftman, A., Angiari, S., Hester, S., Corcoran, S.E., Runtsch, M.C., Ling, C., Ruzek, M.C., Slivka, P.F., McGettrick, A.F., Banahan, K., et al. (2020). The immunomodulatory metabolite itaconate modifies NLRP3 and inhibits inflammasome activation. Cell Metab. *32*, 468–478.e7.

Horvat, J.C., Beagley, K.W., Wade, M.A., Preston, J.A., Hansbro, N.G., Hickey, D.K., Kaiko, G.E., Gibson, P.G., Foster, P.S., and Hansbro, P.M. (2007). Neonatal chlamydial infection induces mixed T-cell responses that drive allergic airway disease. Am. J. Respir. Crit. Care Med. *176*, 556–564.

Italiani, P., and Boraschi, D. (2014). From monocytes to M1/M2 macrophages: phenotypical vs. functional differentiation. Front. Immunol. *5*, 514.

Jaiswal, A.K., Yadav, J., Makhija, S., Mazumder, S., Mitra, A.K., Suryawanshi, A., Sandey, M., and Mishra, A. (2021). Irg1/itaconate metabolic pathway is a crucial determinant of dendritic cells immune-priming function and contributes to resolute allergen-induced airway inflammation. Mucosal Immunol. 2021. Published online October 20. https://doi.org/10.1038/s41385-021-00462-y.

Jha, A.K., Huang, S.C.C., Sergushichev, A., Lampropoulou, V., Ivanova, Y., Loginicheva, E., Chmielewski, K., Stewart, K.M., Ashall, J., Everts, B., et al. (2015). Network integration of parallel metabolic and transcriptional data reveals metabolic modules that regulate macrophage polarization. Immunity *42*, 419–430.

Jiang, H., Harris, M.B., and Rothman, P. (2000). IL-4/IL-13 signaling beyond JAK/STAT. J. Allergy Clin. Immunol. *105*, 1063–1070.

Junttila, I.S. (2018). Tuning the cytokine responses: an update on interleukin (IL)-4 and IL-13 receptor complexes. Front. Immunol. *9*, 888.

Kim, R.Y., Horvat, J.C., Pinkerton, J.W., Starkey, M.R., Essilfie, A.T., Mayall, J.R., Nair, P.M., Hansbro, N.G., Jones, B., Haw, T.J., et al. (2017a). MicroRNA-21 drives severe, steroid-insensitive experimental asthma by amplifying phosphoinositide 3-kinase–mediated suppression of histone deacetylase 2. J. Allergy Clin. Immunol. *139*, 519–532.

Kim, R.Y., Pinkerton, J.W., Essilfie, A.T., Robertson, A.A.B., Baines, K.J., Brown, A.C., Mayall, J.R., Ali, M.K., Starkey, M.R., Hansbro, N.G., et al. (2017b). Role for NLRP3 inflammasome-mediated, IL-1β-dependent responses in severe, steroid-resistant asthma. Am. J. Respir. Crit. Care Med. *196*, 283–297.

Kobayashi, E.H., Suzuki, T., Funayama, R., Nagashima, T., Hayashi, M., Sekine, H., Tanaka, N., Moriguchi, T., Motohashi, H., Nakayama, K., et al. (2016). Nrf2 suppresses macrophage inflammatory response by blocking proinflammatory cytokine transcription. Nat. Commun. *7*, 11624.

Kornberg, M.D., Bhargava, P., Kim, P.M., Putluri, V., Snowman, A.M., Putluri, N., Calabresi, P.A., and Snyder, S.H. (2018). Dimethyl fumarate targets GAPDH and aerobic glycolysis to modulate immunity. Science *360*, 449–453.

Kuljanin, M., Mitchell, D.C., Schweppe, D.K., Gikandi, A.S., Nusinow, D.P., Bulloch, N.J., Vinogradova, E.V., Wilson, D.L., Kool, E.T., Mancias, J.D., et al. (2021). Reimagining high-throughput profiling of reactive cysteines for cell-based screening of large electrophile libraries. Nat. Biotechnol. *39*, 630–641.

Kuo, P.C., Weng, W.T., Scofield, B.A., Paraiso, H.C., Brown, D.A., Wang, P.Y., Yu, I.C., and Yen, J.H. (2020). Dimethyl itaconate, an itaconate derivative, exhibits immunomodulatory effects on neuroinflammation in experimental autoimmune encephalomyelitis. J. Neuroinflammation *17*, 138.

Lampropoulou, V., Sergushichev, A., Bambouskova, M., Nair, S., Vincent, E.E., Loginicheva, E., Cervantes-Barragan, L., Ma, X., Huang, S.C.C., Griss, T., et al. (2016). Itaconate links inhibition of succinate dehydrogenase with macrophage metabolic remodeling and regulation of inflammation. Cell Metab *24*, 158–166.

Langston, P.K., Shibata, M., and Horng, T. (2017). Metabolism supports macrophage activation. Front. Immunol. *8*, 61.

Li, R., Zhang, P., Wang, Y., and Tao, K. (2020). Itaconate: a metabolite regulates inflammation response and oxidative Stress. Oxid. Med. Cell. Longev. *2020*, 5404780.

Liao, S.T., Han, C., Xu, D.Q., Fu, X.W., Wang, J.S., and Kong, L.Y. (2019). 4-Octyl itaconate inhibits aerobic glycolysis by targeting GAPDH to exert anti-inflammatory effects. Nat. Commun. *10*, 5091.

Liu, P.S., Wang, H., Li, X., Chao, T., Teav, T., Christen, S., Di Conza, G., Cheng, W.C., Chou, C.H., Vavakova, M., et al. (2017). α-ketoglutarate orchestrates macrophage activation through metabolic and epigenetic reprogramming. Nat. Immunol. *18*, 985–994.

Lupardus, P.J., Ultsch, M., Wallweber, H., Bir Kohli, P.B., Johnson, A.R., and Eigenbrot, C. (2014). Structure of the pseudokinase-kinase domains from protein kinase TYK2 reveals a mechanism for Janus kinase (JAK) autoinhibition. Proc. Natl. Acad. Sci. USA *111*, 8025–8030.

Mantovani, A., Sozzani, S., Locati, M., Allavena, P., and Sica, A. (2002). Macrophage polarization: tumor-associated macrophages as a paradigm for polarized M2 mononuclear phagocytes. Trends Immunol *23*, 549–555.

Martinez, F.O., and Gordon, S. (2014). The M1 and M2 paradigm of macrophage activation: time for reassessment. F1000Prime Rep. *6*, 13.

Mills, E.L., Ryan, D.G., Prag, H.A., Dikovskaya, D., Menon, D., Zaslona, Z., Jedrychowski, M.P., Costa, A.S.H., Higgins, M., Hams, E., et al. (2018). Itaconate is an anti-inflammatory metabolite that activates Nrf2 via alkylation of KEAP1. Nature *556*, 113–117.

Nelson, V.L., Nguyen, H.C.B., Garcìa-Cañaveras, J.C., Briggs, E.R., Ho, W.Y., Dispirito, J.R., Marinis, J.M., Hill, D.A., and Lazar, M.A. (2018). PPARγ is a nexus controlling alternative activation of macrophages via glutamine metabolism. Genes Dev *32*, 1035–1044.

O'Neill, L.A.J., and Artyomov, M.N. (2019). Itaconate: the poster child of metabolic reprogramming in macrophage function. Nat. Rev. Immunol. *19*, 273–281.

Ogger, P.P., Albers, G.J., Hewitt, R.J., O'Sullivan, B.J., Powell, J.E., Calamita, E., Ghai, P., Walker, S.A., McErlean, P., Saunders, P., et al. (2020). Itaconate controls the severity of pulmonary fibrosis. Sci. Immunol. *5*, eabc1884.

Olagnier, D., Farahani, E., Thyrsted, J., Blay-Cadanet, J., Herengt, A., Idorn, M., Hait, A., Hernaez, B., Knudsen, A., Iversen, M.B., et al. (2020). SARS-CoV2-mediated suppression of NRF2-signaling reveals potent antiviral and anti-inflammatory activity of 4-octyl-itaconate and dimethyl fumarate. Nat. Commun. *11*, 4938.

Puchalska, P., Huang, X., Martin, S.E., Han, X., Patti, G.J., and Crawford, P.A. (2018). Isotope tracing untargeted metabolomics reveals macrophage polarization-state-specific metabolic coordination across intracellular compartments. iScience *9*, 298–313.

Qin, W., Qin, K., Zhang, Y., Jia, W., Chen, Y., Cheng, B., Peng, L., Chen, N., Liu, Y., Zhou, W., et al. (2019). S-glycosylation-based cysteine profiling reveals regulation of glycolysis by itaconate. Nat. Chem. Biol. *15*, 983–991.

Qin, W., Zhang, Y., Tang, H., Liu, D., Chen, Y., Liu, Y., and Wang, C. (2020). Chemoproteomic profiling of itaconation by bioorthogonal probes in inflammatory macrophages. J. Am. Chem. Soc. *142*, 10894–10898.

Rőszer, T. (2015). Understanding the mysterious M2 macrophage through activation markers and effector mechanisms. Mediators Inflamm *2015*, 816460.

Ryan, D.G., Murphy, M.P., Frezza, C., Prag, H.A., Chouchani, E.T., O'Neill, L.A., and Mills, E.L. (2019). Coupling Krebs cycle metabolites to signalling in immunity and cancer. Nat. Metab. *1*, 16–33.

Schwartz, D.M., Kanno, Y., Villarino, A., Ward, M., Gadina, M., and O'Shea, J.J. (2017). JAK inhibition as a therapeutic strategy for immune and inflammatory diseases. Nat. Rev. Drug Discov. *16*, 843–862.

Sica, A., and Mantovani, A. (2012). Macrophage plasticity and polarization: in vivo veritas. J. Clin. Invest. *122*, 787–795.

Siu, T., Brubaker, J., Fuller, P., Torres, L., Zeng, H., Close, J., Mampreian, D.M., Shi, F., Liu, D., Fradera, X., et al. (2017). The discovery of 3-((4-chloro-3-methoxyphenyl)amino)-1-((3R,4S)-4-cyanotetrahydro-2H-pyran-3-yl)-1H-pyrazole-4-carboxamide, a highly ligand efficient and efficacious Janus kinase 1 selective inhibitor with favorable pharmacokinetic properties. J. Med. Chem. *60*, 9676–9690.

Smith, J.K., Patil, C.N., Patlolla, S., Gunter, B.W., Booz, G.W., and Duhé, R.J. (2012). Identification of a redox-sensitive switch within the JAK2 catalytic domain. Free Radic. Biol. Med. *52*, 1101–1110.

Szanto, A., Balint, B.L., Nagy, Z.S., Barta, E., Dezso, B., Pap, A., Szeles, L., Poliska, S., Oros, M., Evans, R.M., et al. (2010). STAT6 transcription factor is a facilitator of the nuclear receptor PPARγ-regulated gene expression in macrophages and dendritic cells. Immunity *33*, 699–712.

Toms, A.V., Deshpande, A., McNally, R., Jeong, Y., Rogers, J.M., Kim, C.U., Gruner, S.M., Ficarro, S.B., Marto, J.A., Sattler, M., et al. (2013). Structure of a pseudokinase-domain switch that controls oncogenic activation of Jak kinases. Nat. Struct. Mol. Biol. *20*, 1221–1223.

Viola, A., Munari, F., Sánchez-Rodríguez, R., Scolaro, T., and Castegna, A. (2019). The metabolic signature of macrophage responses. Front. Immunol. *10*, 1462.

Wadhwa, R., Dua, K., Adcock, I.M., Horvat, J.C., Kim, R.Y., and Hansbro, P.M. (2019). Cellular mechanisms underlying steroid-resistant asthma. Eur. Respir. Rev. *28*, 190096.

Wang, F., Zhang, S., Vuckovic, I., Jeon, R., Lerman, A., Folmes, C.D., Dzeja, P.P., and Herrmann, J. (2018). Glycolytic stimulation is not a requirement for M2 macrophage differentiation. Cell Metab *28*, 463–475.e4.

Weiss, J.M., Davies, L.C., Karwan, M., Ileva, L., Ozaki, M.K., Cheng, R.Y.S., Ridnour, L.A., Annunziata, C.M., Wink, D.A., and McVicar, D.W. (2018). Itaconic acid mediates crosstalk between macrophage metabolism and peritoneal tumors. J. Clin. Invest. *128*, 3794–3805.

Willenborg, S., Sanin, D.E., Jais, A., Ding, X., Ulas, T., Nüchel, J., Popović, M., MacVicar, T., Langer, T., Schultze, J.L., et al. (2021). Mitochondrial metabolism coordinates stage-specific repair processes in macrophages during wound healing. Cell Metab *33*, 2398–2414.e9.

Xu, T., Park, S.K., Venable, J.D., Wohlschlegel, J.A., Diedrich, J.K., Cociorva, D., Lu, B., Liao, L., Hewel, J., Han, X., et al. (2015). ProLuCID: an improved SEQUEST-like algorithm with enhanced sensitivity and specificity. J. Proteomics *129*, 16–24.

Yang, C., Liu, T., and Shi, G.P. (2020). Therapeutic potential of tricarboxylic acid cycle metabolite itaconate in cardiovascular diseases. EBiomedicine *59*, 102938.

Zhang, Y., Qin, W., Liu, D., Liu, Y., and Wang, C. (2021). Chemoproteomic profiling of itaconations in: *Salmonella*. Chem. Sci. *12*, 6059–6063.

Zhu, K., Borrelli, K.W., Greenwood, J.R., Day, T., Abel, R., Farid, R.S., and Harder, E. (2014). Docking covalent inhibitors: a parameter free approach to pose prediction and scoring. J. Chem. Inf. Model. *54*, 1932–1940.

STAR★METHODS

KEY RESOURCES TABLE

REAGENT or RESOURCE	SOURCE	IDENTIFIER
Antibodies		
Anti-β-actin	Sigma	Cat# A5316; RRID: AB_476743
Anti-NRF2	Cell Signaling	Cat# 12721S; RRID: AB_2715528
Anti-Phospho-Stat6 (Tyr641)	Cell Signaling	Cat# 56554S; RRID: AB_2799514
Anti-Stat6	Cell Signaling	Cat# 9362S; RRID: AB_2271211
Anti-Phospho-Jak1 (Tyr1034/1035)	Cell Signaling	Cat# 3331S; RRID: AB_2265057
Anti-Jak1	Cell Signaling	Cat# 3332S; RRID: AB_2128499
Anti-SOCS1 (A156)	Cell Signaling	Cat# 3950T
Anti-Phospho-Stat1 (Tyr701) (58D6)	Cell Signaling	Cat# 9167S; RRID: AB_561284
Anti-Stat1	Cell Signaling	Cat# 9172S; RRID: AB_2198300
Purified Rat Anti-Mouse CD16/CD32 (Mouse BD Fc Block)	Biolegend	Cat # 553141; RRID: AB_394656
PE anti-mouse CD206 (MMR)	Biolegend	Cat# 141706; Clone C068C2
APC anti-mouse CD301 (MGL1/MGL2)	Biolegend	Cat# 145708; Clone LOM-14
PE anti-mouse CD124 (IL-4Rα)	Biolegend	Cat# 144804; Clone I015F8
PerCP/Cyanine5.5 anti-mouse F4/80	Biolegend	Cat# 123128; Clone BM8
PE anti-mouse IL-13	Biolegend	Cat# 159403; Clone W17010B
*nVivo*MAb anti-mouse IL-4	Bio X Cell	Cat# BE0045; Clone 11B11
Hamster anti-mouse CD3 (clone 145-2C11)	BD Biosciences	Cat #: 553057; RRID: AB_394590
Hamster anti-mouse CD28 (clone 37.51)	Tonbo Biosciences	Cat# 70-0281; RRID: AB_2621492
Rat anti-mouse IFN-γ (clone XMG1.2)	BD Biosciences	Cat# 554408; RRID: AB_395373
Phospho-tyrosine-specific antibody PT66K	Cisbio	Cat# 61T66KLA and 61T66KLB
ANTI-FLAG M2 antibody	Sigma Aldrich	Cat# F3165
Bacterial and virus strains		
C. muridarum (Cmu) (VR-123)	ATCC	Cat# ATCC CRL-1696
Biological samples		
Blood samples from healthy donors	School of Biochemistry and Immunology, TCD	N/A
Chemicals, peptides, and recombinant proteins		
4-Octyl Itaconate	Professor Richard Hartley, University of Glasgow	N/A
Itaconic Acid	Sigma	Cat# I29204
Lymphoprep	StemCell Technologies	Cat# 07861
Recombinant Human M-CSF	Peprotech	Cat# 300-25
Pacific Blue Annexin V Apoptosis Detection Kit with PI	Biolegend	Cat# 640928
CD62L MicroBeads, mouse	Miltenyi Biotec	Cat# 130-049-701
WesternBright ECL	Advansta	Cat# K-12049-D50
PMA	Sigma Aldrich	Cat# P8139; CAS:16561-29-8
Ionomycin	Sigma Aldrich	Cat# I0634; CAS: 56092-82-1
Brefeldin A	Sigma Aldrich	Cat# B7651; CAS: 20350-15-6
Fixation Buffer	BioLegend	Cat# 420801
Intracellular Staining Permeabilization Wash Buffer (10X)	BioLegend	Cat# 421002
(2-Hydroxypropyl)-b-cyclodextrin	Sigma Aldrich	Cat# H107; CAS: 128446-35-5
Recombinant Mouse IL-4 (carrier-free)	Biolegend	Cat# 574306
Recombinant Mouse IL-13 (carrier-free)	Biolegend	Cat# 575904
Recombinant Mouse IFN-β1 (carrier-free)	Biolegend	Cat# 581304

(*Continued on next page*)

Continued

REAGENT or RESOURCE	SOURCE	IDENTIFIER
Recombinant Mouse IFN-γ (carrier-free)	Biolegend	Cat# 575306
Dimethyl 2-oxoglutarate (DM-αKG)	Sigma-Aldrich	Cat# 349631
Recombinant Murine IL-4	Peprotech	Cat# 214-14
Ovalbumin (323-339)	Sigma-Aldrich	Cat# O1641
Alhydrogel adjuvant 2%	Jomar Life Research	Cat# vac-alu-250
Dexamethasone	Sigma Aldrich	Cat# D4902-500MG; CAS 50-02-2
4-Octyl Itaconate	Sigma Aldrich	Cat# SML2338-25MG; CAS 3133-16-2
Halt Protease Inhibitor Cocktail (100X)	Thermo Fisher Scientific	Cat# 78430
SuperSignal West Femto Maximum Sensitivity Substrate	Thermo Fisher Scientific	Cat# 34095
Seahorse XF Medium	Agilent	Cat# 103575
JAK1 Kinase Domain	AbbVie	N/A
Tofacitinib	AbbVie	N/A
Ruxolitinib	AbbVie	N/A
Staurosporine	AbbVie	N/A
Streptavidin-Allophycocyanin	Aglient (Formerly ProZyme)	PJ27S
ATP	Promega	Cat# P1132
Lipofectamine 2000	ThermoFisher	Cat# 11668030
Itaconate-alkyne (ITalk)	Professor Chu Wang, Peking University	Qin et al. (2020)
TBTA ligand	Strem	Cat# 07-3215
Biotin-Azide	ChemPep	Cat# 271604
Tris(2-carboxyethyl)phosphine hydrochloride (TCEP)	Sigma Aldrich	Cat# 4706
Streptavidin-agarose beads	Thermo Fisher Scientific	Cat# 20353
CD14 MicroBeads, human	Miltenyi Biotec	Cat# 130-050-201
Pierce Streptavidin Plus Ultralink beads	Thermo Fisher Scientific	Cat# PI53116
Critical commercial assays		
PureLink RNA Mini Kit	Invitrogen	Cat# 12183025
High-Capacity cDNA Reverse Transcription Kit	Applied Biosystems	Cat# 4368814
PowerUp SYBR Green Master Mix	Applied Biosystems	Cat# A25743
Seahorse XF Cell Mito Stress Test Kit	Agilent	Cat# 103015-100
CD4+ T Cell Isolation Kit, mouse	Miltenyi Biotec	Cat# 130-104-454
Seahorse XFe96 FluxPak	Agilent	Cat# 102416–100
Pierce High pH Reversed-Phase Peptide Fractionation Kit	Thermo Fisher Scientific	Cat# 84868
Experimental models: Cell lines		
Human: HEK293T cells	Sigma	Cat# 12022001
Human: THP-1 cells	ATCC	Cat# TIB-202
Experimental models: Organisms/strains		
Mouse: C57BL/6JOlaHsd	Harlan UK	N/A
Mouse: BALB/c	Phil Hansbro Laboratory, University of Newcastle	N/A
Mouse: NFE2L2$^{-/-}$	Albena Dinkova-Kostova Lab, University of Dundee	N/A
Oligonucleotides		
18s Primer: F (5'-3'): GTAACCCGTTGAACCCC ATT; R (5'-3'): CCATCCAATCGGTAGTAGGG	This paper	N/A
Fizz1 Primer: F (5'-3'): ACCTTTCCTGAGATTCTGC CCC; R (5'-3'): CAGTGGTCCAGTCAACGAGTAAGC	This paper	N/A
Arg1 Primer: F (5'-3'): TGACATCAACACTCCCCTGA CAAC; R (5'-3'): GCCTTTTCTTCCTTCCCAGCAG	This paper	N/A

(*Continued on next page*)

Continued

REAGENT or RESOURCE	SOURCE	IDENTIFIER
Mrc1 Primer: F (5'-3'): TCTTTTACGAGAAGTTGGG GTCAG; R (5'-3'): ATCATTCCGTTCACCAGAGGG	This paper	N/A
Pparg Primer: F (5'-3'): ACGATCTGCCTGAGGT CTGT; R (5'-3'): CATCGAGGACATCCAAGACA	This paper	N/A
Ym1 Primer: F (5'-3'): GGCTACACTGGAGAAAAT AGTC CCC; R (5'-3'): CCAACCCACTCATTACCCTGATAG	This paper	N/A
Tbp Primer: F (5'-3'): CCGTGAATCTTGGCTGTA AAC; R (5'-3'): TGTCCGTGGCTCTCTTATTC	This paper	N/A
Il13 Primer: F (5'-3'): GCTGAGCAACATCACAC AAG; R (5'-3'): AATCCAGGGCTACACAGAAC	This paper	N/A
Il5 Primer: F (5'-3'): GCTTCCTGTCCCTACTCATAAA; R (5'-3'): CCCACGGACAGTTTGATTCT	This paper	N/A
Recombinant DNA		
JAK1 cDNA ORF Clone, Rat, C-DYKDDDDK (Flag) tag	Sino Biological	RG81640-CF
Software and algorithms		
Image Lab (Version 6.1)	Bio-Rad	https://www.bio-rad.com/
FlowJo v 10.7	FlowJo	https://www.flowjo.com/
Graphpad Prism 9.0	Graphpad	https://www.graphpad.com/
Seahorse Wave Controller Software (version 2.4.2)	Agilent	https://www.agilent.com/
ImageJ	NIH	https://imagej.nih.gov/ij/
ProLuCID	Xu et al. (2015)	http://fields.scripps.edu/yates/wp/?page_id=821
pFind	Chi et al. (2018)	http://pfind.ict.ac.cn/software/pFind3/index.html
MaxQuant 1.6.15.0	Max Planck Institute of Biochemistry	https://www.maxquant.org/
MAESTRO	Schrödinger	https://www.schrodinger.com/products/maestro
CovDock	Schrödinger	https://www.schrodinger.com/science-articles/covdock
Other		
UltiMate 3000 Nano-LC system	Thermo Fisher Scientific	Cat# ULTIM3000RSLCNANO
FlexiVent apparatus (FX1 System)	SCIREQ	https://www.scireq.com/flexivent/

RESOURCE AVAILABILITY

Lead contact

Further information and requests for resources and reagents should be directed to and will be fulfilled by the lead contact, Professor Luke A.J. O'Neill (laoneill@tcd.ie).

Materials availability

This study did not generate new unique reagents.

Data and code availability

All data reported in this paper will be shared by the lead contact upon request. This paper does not report original code. Any additional information required to reanalyze the data reported in this paper is available from the lead contact upon request.

EXPERIMENTAL MODEL AND SUBJECT DETAILS

Mice

6-8 weeks old C57Bl/6J female mice (Harlan UK) were used to isolate murine bone marrow- derived macrophages and splenic T cells. Mice were bred and housed in the Comparative Medicine Unit (CMU) in Trinity Biomedical Sciences Institute (TBSI) (Trinity

College Dublin, TCD, Ireland). All mice were maintained under specific pathogen-free conditions according to Irish and European Union regulations. All the procedures involving experiments on animals have been approved by the Health Products Regulatory Authority (HPRA, Ireland), and were conducted according to Directive 2010/63/EU of the European Parliament and Council on the protection of animals used for scientific purposes. Legs of Nfe2l2-/- (NRF2-null) and matched WT mice were kindly donated by Professor Albena Dinkova-Kostova and Elena Knatko at University of Dundee, Scotland.

Murine bone marrow-derived macrophage (BMDM) culture

Bone marrow was obtained by flushing DMEM media through the femur, tibia, and hip bone of mice with a 25-gauge needle. The bone marrow was subsequently resuspended in red cell lysis buffer (Sigma) for 3 minutes before being centrifuged, resuspended, and passed through a 70 μm cell strainer. Cells were plated in 10 cm petri dishes and in DMEM media containing L-glutamine (Gibco) supplemented with FCS (10%) (Sigma-Aldrich), penicillin-streptomycin (1%) (Sigma-Aldrich) and L929 supernatant (10%) and cultured at 37°C in a 5% CO_2 incubator for 6 days. On day 6, cells were scraped, resuspended in DMEM complete media, and seeded into multiwell plates at $5x10^5$ or $1x10^6$ cells/mL.

Macrophage activation

BMDMs were seeded in 12-well plates and left overnight at 37°C in 5% CO_2 incubator. 1 hour prior to treatment, BMDMs were resuspended in serum-free DMEM media. Cells were treated with recombinant mouse IL-4 (20 ng/mL, Biolegend) for 5 min to 24h, as noted in the figure legends/results. For IL-13 stimulations of BMDMs, 20 ng/mL recombinant mouse IL-13 was used (Biolegend). Recombinant mouse IFN-β1 (Biolegend) and IFNγ (Biolegend) were used at 20 ng/mL.

Treatment of cells with OI and itaconate

4-octyl itaconate (OI) was originally synthesized and kindly provided by the laboratory of Professor Richard Hartley, University of Glasgow, Scotland. Experimental observations were confirmed using OI purchased from commercial suppliers (Fluorochem and Sigma). OI was prepared at a concentration of 250 mM in DMSO and used at a working concentration of 250 μM, unless otherwise noted. For all *in vitro* experiments with OI, DMSO was used as a vehicle control. Itaconic acid (Sigma-Aldrich) was prepared in DMEM media (Gibco) at a concentration of 5 mM, and pH was brought to 7.4 using 1 M NaOH. Both control and itaconate media were then sterilized using a 0.2 μm filter and added directly to BMDMs. BMDMs were pretreated with OI or itaconate for 2 hours before cytokine stimulation. For dimethyl 2-oxoglutarate (DM-αKG, Sigma-Aldrich 349631), cells were treated at a concentration of 1 mM.

T Cell isolation and culture

Murine resting T cells were purified from total mouse splenocytes by magnetic cell sorting with a $CD4^+$ T Cell Isolation Kit (Miltenyi), followed by incubation with CD62L microbeads, all according to manufacturer's instructions (all reagents from Miltenyi Biotech). Cells were stimulated *in vitro* with plate-bound anti-CD3 and anti-CD28 antibodies (1 mg/ml and 2 mg/ml, respectively; BD Biosciences) + 40 ng/ml IL-4 (Biolegend) + 5 μg/ml anti-mouse IFN-g antibody (BD Biosciences) in RPMI 1640 containing L-glutamine (Gibco), supplemented with 10% heat-inactivated fetal bovine serum (Sigma-Aldrich), 55 mM 2-mercaptoethanol (Gibco) and 100 U/ml penicillin/streptomycin (Sigma-Aldrich). For experiments with OI, cells were pre-incubated at 37°C for 30 min with OI at 125 μM or 250 μM, or equal amounts of DMSO (control condition) before activation. For experiments with itaconate, cells were pre-incubated at 37°C for 30 min with 2.5 mM or 5 mM itaconate pH 7.4

In vivo IL-4 complex murine model

IL-4–anti–IL-4 mAb complex (IL-4c) was prepared as described previously by Finkelman and colleagues (Finkelman et al., 1993). Briefly, 5 μg of recombinant murine IL-4 (PeproTech) was incubated with 25 μg 11B11 (Bio X Cell) for 10 minutes on ice to allow for antibody-cytokine complex to form, then diluted in PBS. Female, 6-8 weeks old, C57BL/6 WT mice were then intraperitoneally injected with OI 50 mg/kg dissolved in PBS/40% cyclodextrin or PBS/cyclodextrin alone (vehicle control) for 3 hours. Mice were then injected with IL-4c or PBS (control). For JAK1/STAT6 Western blot analysis, PECs were collected 5 and 24 hours after IL-4c injection, counted, and lysed in Laemmli buffer containing 10mM Na_3VO_4. We determined that JAK1/STAT6 phosphorylation was highest in WT control mice 5 hours after IL-4c injection, and thus collected PECs from OI and control-treated mice using the 5-hour time point. For mRNA analysis, OI and IL-4c injections were repeated on day 2, and PECs were collected on day 4. PECs were pelleted, red blood cell-lysed, and lysed in RNA lysis buffer (Invitrogen).

Experimental asthma infection murine model

Murine models of ovalbumin (Ova)-induced allergic airway disease and Chlamydia respiratory infections were combined to induce severe steroid-resistant allergic airway disease as previously described (Essilfie et al., 2015; Kim et al., 2017a, 2017b). Briefly, female wild-type BALB/c mice, 6-8 weeks old, were sensitized to Ova (50μg intraperitoneal [i.p.] injection, Sigma-Aldrich, Sydney, Australia) in Th2-inducing adjuvant aluminium hydroxide (Alhydrogel, 2%, Jomar) in sterile saline (200μl). They were subsequently challenged intranasally (i.n.) with Ova (10μg/50μL sterile saline) on day 12-13 and again on day 33-34. Mice were then inoculated under isoflurane anesthesia on day 14 i.n. with *C. muridarum* (Cmu) (ATCC VR-123), 100 inclusion-forming units, in 30μL sucrose phosphate glutamate [SPG] buffer. Sham-sensitized controls received saline sensitization with Alhydrogel and the subsequent Ova challenges. AAD was

characterized on day 35. Some mice were treated with dexamethasone (DEX) (2mg/kg, Sigma-Aldrich) i.n. or 4-octyl itaconate (OI) (5mg/kg i.n.) on day 32-34.

Lung function (airway resistance or Rn) was measured by anesthetizing mice with ketamine (100mg/kg) and xylazine (10mg/kg, Troy Laboratories, Smithfield, Australia) and cannulating their tracheas (tracheostomy with ligation). FlexiVent apparatus (FX1 System, SCIREQ, Montreal, Canada) was used to assess airway-specific resistance (Rn, tidal volume of 8mL/kg at a respiratory rate of 450 breaths/min) in response to increasing doses of nebulized methacholine (Sigma-Aldrich). Assessments were performed at least three times per dose of saline/methacholine and the average calculated.

Mice were sacrificed on day 35, and their lungs were flash-frozen. Lung tissue was then used for subsequent RNA extraction or protein isolation for qPCR and immunoblot analysis, respectively. Macrophage counts were obtained from May Grunwald Giemsa stained bronchoalveolar lavage fluid cells using a light microscope (Essilfie et al., 2015; Kim et al., 2017a, 2017b).

METHOD DETAILS

RNA extraction and qPCR

Media supernatant was removed, cells were washed with PBS and lysed in 350 μL RNA lysis buffer (Invitrogen). One volume 70% EtOH was added before transferring to Invitrogen RNA spin columns. The purification was followed as per manufacturer's instructions (Invitrogen PureLink RNA kit, ThermoFisher). Eluted RNA was quantified using a Nanodrop 2000 spectrophotometer and each RNA sample was diluted to the lowest yield before reverse-transcriptase PCR. cDNA was prepared using the High Capacity cDNA Reverse Transcription kit (Applied Biosystems), according to manufacturer's instructions. qRT-PCR was then performed using the PowerUp SYBR Green Master on a 7500 Fast thermocycler (Applied Biosystems), and Ct values were converted to 2^(-ΔΔCt) using the Ct of the housekeeping gene *18s* (BMDMs) or *Tbp* ($CD4^+$ T cells).

Western blotting

Media supernatant was removed, and cells were lysed in 5x Laemmli Sample Buffer containing 10mM Na_3VO_4 or HALT Protease Inhibitor Cocktail (Thermo Scientific) and heated at 95°C for 5 minutes. Protein samples were resolved on SDS-PAGE gels and transferred onto a polyvinylidene difluoride (PVDF) membrane via wet transfer. Membranes were probed with primary antibodies at a 1:1000 dilution (or 1:10000 for β-actin) and secondary HRP-conjugated antibodies at a 1:2000 dilution. Membranes were visualized using WesternBright ECL HRP substrate (Advansta) or SuperSignal West Femto Maximum Sensitivity Substrate (Thermo Scientific) on a GelDoc system (Bio-Rad). Images were analyzed with ImageLab (Bio-Rad) and ImageJ software. β-actin was used as reference housekeeping protein.

Flow cytometry

BMDM media supernatant was removed, cells were washed with PBS and then removed using a cell scraper. Macrophages were then treated with Fcγ-blocking antibody anti-mouse CD16/32 (Biolegend, clone 93) for 10 minutes, before they were stained with fluorochrome-conjugated antibodies for surface proteins in FACS buffer. The antibodies used were: PerCP/Cy5.5 anti-mouse F4/80 1:1000 (clone BM8, Biolegend), APC anti-mouse CD301 (MGL1/MGL2) 1:250 (clone LOM-14, Biolegend), PE anti-mouse CD206 1:250 (clone C068C2, Biolegend), PE anti-mouse CD124 (IL-4Ra) 1:250 (clone I015F8, Biolegend). To analyze BMDM expression of M2 surface markers, cells were first gated on $F4/80^+$ followed by CD206, CD301, or CD124. For annexin V/PI staining to measure cell death, cells were scraped and washed with PBS, then resuspended in cold annexin V binding buffer (Biolegend). Anti-annexin V Pacific Blue (Biolegend) and propidium iodide (PI) (Invitrogen) were added according to manufacturer's instructions (Annexin V Apoptosis Detection Kit, Biolegend). Cells were incubated for 15 minutes, then additional annexin V binding buffer was added, and cells were run on the flow cytometer. For intracellular cytokine staining in $CD4^+$ T cells, cells were collected, washed, and re-stimulated with 50 ng/ml phorbol 12-myristate 13-acetate (PMA) + 1 μg/ml ionomycin + 10 μg/ml brefeldin A (all from Sigma Aldrich). After 4 hours, cells were washed, fixed/permeabilized with fixation and permeabilization buffers (BioLegend) and stained with anti-mouse IL-13 (Biolegend). All samples were analyzed on a FACS Canto II Cell analyzer (BD Biosciences). Analysis of acquired data was performed with the FlowJo software (FlowJo LLC).

Seahorse metabolic assays

Mito Stress Tests were performed to measure oxygen consumption rate (OCR) of BMDMs using the Agilent Seahorse XF Cell Mito Stress Test Kit and system, according to manufacturer's instructions. Briefly, 50,000 or 100,000 cells per well were seeded overnight in a 96-well XF Cell Culture Microplate (Agilent) in DMEM medium containing DMEM media containing L-glutamine (Gibco) supplemented with FCS (10%) (Sigma-Aldrich), penicillin-streptomycin (1%) (Sigma-Aldrich). The morning of the assay, DMEM was removed, and cells were washed twice with Seahorse XF Base Medium (Agilent). XF Base medium containing 25 mM glucose, 2 mM L-glutamine, and 1 mM sodium pyruvate was then added and cells were left in a CO_2-free incubator for 1 h prior to the assay. OCR was measured on a Seahorse XF Analyser (Agilent). OCR was measured at three timepoints each, in basal conditions and following the addition of oligomycin (1.0 μM), carbonyl cyanide-4-(trifluoromethoxy)phenylhydrazone (FCCP; 1.0 μM), and rotenone/antimycin A (both at 0.5 μM) (all from Agilent Seahorse XF Cell Mito Stress Test Kit), to determine maximum respiration and spare respiratory capacity of tested cells. Data was analyzed using the Seahorse XF software.

JAK1 kinase enzymatic activity assay

Jak1 kinase activity was measured biochemically using a kinase domain construct from an AbbVie in-house preparation. The reaction buffer contains 50mM MOPSO, pH 6.5, 10 mM $MgCl_2$, 2 mM $MnCl_2$, 0.1% BSA, 0.1 mM Na_3VO_4, and 2.5 mM DTT. A mixture containing final concentrations of 2 μM biotinylated-Fibroblast Growth Factor Receptor (bio-FGFR) peptide substrate (LCBiot-(Ahx)AEEEYFFLFA-amide) (New England Peptide), 3.1 nM Jak1 kinase domain, 5% DMSO (Sigma) and a dose response of itaconate, OI (Sigma), tofacitinib, ruxolitinib, and staurosporine (AbbVie) was pre-incubated for one-hour at room temperature. The reaction was initiated with 1 μM final concentration of ATP (Promega) and incubated for one hour at room temperature. The reaction was quenched using 10 μL of 0.5 M EDTA, pH 7.5. Phosphorylated bio-FGFR was detected using a revelation buffer of 50mM HEPES, 400mM KF, 0.01% Tween-20, 0.1% BSA (all Sigma) supplemented with 11.3 ng/well phospho-tyrosine-specific antibody PT66K (Cisbio) and 78 ng/well PhycoLink Streptavidin-APC (SAXL) (Prozyme). The reaction plate was stored at 4°C overnight and read on a PHERAstar plate reader using FRET settings with an excitation wavelength of 337nm and emission wavelengths of 620nm and 665nm.

Validation of ITalk labeling of JAK1

HEK293T cells were grown to 50% confluence in 15 cm dishes, then transfected with PCMV3-ORF-FLAG-JAK1 plasmid (Sino Biological) using Lipofectamine2000 for 24 hours, according to manufacturer's instructions. Subsequently, the cells were treated with 100 μM ITalk or DMSO for 12 hours. The cells were washed with PBS three times and centrifuged at 1000 rpm for 3 min. The cell pellets were stored at -80°C. Cell pellets were then resuspended in 1 ml ice-cold PBS containing EDTA-free Pierce Halt protease inhibitor cocktail. The cells were lysed by sonication on ice and lysates were collected by centrifugation (20,000 g, 30 min) at 4°C to remove debris. Protein concentration was determined by using a BCA protein assay kit. 50 μl lysate (2 mg/ml) was saved for the input portion, and the remaining portion (950 μl lysate, 2 mg/mL) was mixed with 1 mM CuSO4, 100 μM TBTA ligand (Strem, 07-3215), 100 μM Biotin-Azide (ChemPep, 271604) and 1 mM TCEP (Sigma Aldrich, C4706) for 1 hour at room temperature. The resulting click-labeled lysates were centrifuged at 8000 g for 5 min at 4°C and washed twice with 1 mL cold methanol. The proteins were resuspended in 1 mL PBS containing 1.2% SDS via sonication and heating (5 min, 90°C). Samples were then diluted with 5 mL of PBS for a final SDS concentration of 0.2%. The solutions were then incubated with 100 μl of streptavidin-agarose beads (Thermo Fisher Scientific, 20353) for 3 hours at 29°C, followed by washing with 5 mL PBS three times, and 5 mL distilled water three times. 40 μl loading buffer was added in the resulting beads and heated for 10 min (95°C), centrifuged at 2000 g for 3 min and supernatant was collected for eluction input. The input and elution were resolved on 6% SDS-PAGE gels, and JAK1 was detected via Western Blot using monoclonal anti-flag M2 antibody (Sigma, F3165).

Identification of JAK1 modification sites by ITalk

HEK293T cells were grown to 70% confluence in 15 cm dishes, then transfected with PCMV3-ORF-Flagged-JAK1 plasmids using Lipofactamine 2000 for 24 hours. Cells were then washed with PBS three times, centrifuged at 1000 rpm for 3 min and stored at -80 °C. The cell pellets were lysed via sonication in 1 mL ice-cold PBS containing EDTA-free Pierce Halt protease inhibitor cocktail. Cell lysates were collected by centrifugation (20,000 g, 30 min) at 4 °C to remove the debris. Protein concentration was determined via BCA protein assay. 1 mL cell lysates (2 mg/mL) were incubated with 1 mM ITalk in 37 °C for 2 hours, then resulting lysates were precipitated with 4 mL methanol, 1 mL chloroform and 3 mL Milli-Q water. The precipitated proteins were centrifuged at 4000 g for 10 min at 4 °C and washed twice with 500 μL cold methanol and resuspended in 1 mL PBS containing 0.4% SDS. 1 mL cell lysates (2 mg/mL) were then reacted with 1 mM $CuSO_4$, 100 μM TBTA ligand (Strem, 07-3215), 1 mM TCEP (Sigma Aldrich, C4706) and 100 μM acid-cleavable azide-biotin (DADPS Biotin Azide, cat. no. 1330-5) for 1 h at room temperature. The resulting click-labeled lysates were precipitated by 4 mL methanol, 1 mL chloroform and 3 mL Milli-Q water. The precipitated proteins were centrifuged at 4000 g for 10 min at 4 °C, washed twice with 500 μL cold methanol, and then resuspended in 1 mL PBS containing 1.2% SDS. 100 μL streptavidin beads (Thermo Fisher Scientific) were washed three times with 1 mL PBS and resuspended in 5 mL PBS, which was added to the protein solution. The beads were incubated with the protein solution for 4 h at 29°C, then washed with 5 mL PBS three times, then 5 mL distilled water three times. The resulting beads were resuspended in 500 μL PBS containing 6 M urea, incubated in 10 mM DTT at 37 °C for 30 min, and added with 20 mM iodoacetamide for 30 min at 35 °C in the dark. The beads were then collected by centrifugation and resuspended in 200 μL PBS containing 2M urea, 1 mM $CaCl_2$ and 10 ng/uL trypsin (Promega). Trypsin digestion was performed at 37 °C with rotation overnight and the beads were washed with 200 μL distilled water three times. Release of the modified peptides from the beads was carried out by incubating the beads with 200 μL of 2% formic acid/water for 1 h with gentle rotation in 25 °C. After centrifugation, the supernatant was collected. Then the cleavage process was repeated, and supernatant was combined. In addition, the beads were washed with 50% acetonitrile/water containing 1% formic acid (400 μL), and the washes were combined with the supernatant to form the cleavage fraction. Sample was dried in a vacuum centrifuge and stored at -30 °C until LC-MS/MS analysis.

Data analysis of JAK1 modification by ITalk

To identify the modification sites, LC-MS/MS data was analyzed using ProLuCID (Xu et al., 2015) with static modification of cysteine (+57.0215 Da) as well as variable modifications of +325.16378 Da on cysteine. The MS/MS spectra of the peptide containing ITalk modification were generated using the pFind software (Chi et al., 2018).

Profiling of OI modification in human macrophages

Human PBMCs were isolated from human blood using Lymphoprep (Axis-Shield). Whole blood (30 ml) was layered on 20 ml Lymphoprep and spun for 20 min at 2,000 r.p.m. with no brake on. The PBMC layer was isolated and $CD14^+$ monocytes were sorted using magnetic-activated cell sorting (MACS) CD14 beads. Cells were plated at 1×10^6 cells ml^{-1} in RPMI supplemented with 10% (v/v) FCS, 2 mM L-glutamine, and 1% penicillin/streptomycin solution containing M-CSF (50 ng ml^{-1}) and maintained at 37 °C, 5% CO_2 for 6 days, to allow differentiation into macrophages. The macrophages were pre-incubated with DMSO or 125 μM OI for 2 hr prior to incubation with 150 μM ITalk for 2 hr. The cells were trypsinized and pelleted. The cells were lysed in 0.5 mL ice-cold PBS buffer containing EDTA-free Pierce Halt protease inhibitor cocktail with sonication. The cell lysates were collected by centrifugation (20,000 g, 30 min) at 4 °C to remove the debris. The protein concentration was determined by using the BCA protein assay kit. 500 μg cell lysates were reacted with 1 mM CuSO4, 100 μM TBTA ligand, 100 μM azide-biotin, and 1 mM TCEP for 1 h at room temperature. The resulting click-labeled lysates were precipitated by methanol/chloroform and centrifuged at 1400 g for 20 min at 4 °C and washed twice with cold methanol. The proteins were re-solubilized with 6 M urea containing 1% SDS, incubated with 10 mM DTT at 65 °C for 15 min, followed by addition of 20 mM iodoacetamide for 30 min at room temperature in the dark. 100 μL Pierce streptavidin plus ultralink beads (Thermo Fisher Scientific) were washed for three times with 1 mL PBS, and resuspended in 5 mL PBS, which was added to the protein solution. The resulting solution was incubated overnight at 4 °C, followed by washing with 5ml PBS containing 1%SDS for three times, 5 mL PBS for three times, and 5 mL distilled water for three times. The beads were then collected by centrifugation and resuspended in 200 μL 100 mM TEAB buffer (pH 8.5). 0.5 μg of trypsin/Lys-C was added to the beads for overnight digestion at 37 °C with shaking at 500 rpm. TMT-duplex reagents (0.2 mg in each reagent) were resuspended in dry acetonitrile, added to the digested samples, and incubated for 1 hr at room temperature with shaking at 500 rpm. Afterwards, the TMT labeling reaction was terminated by adding 50% hydroxylamine (0.3% final concentration) to the mixture and incubate for 15 min. The labeled peptide samples were dried in speedvac and resuspended in 300 μL 0.1% TFA and subjected to Pierce High pH Reversed-Phase Peptide Fractionation Kit following manufacturer's protocol.

Quantitative profiling of OI modified cysteinome

THP1 cells were seeded into 6 cm petri dishes (4 million per dish) in 5 ml media, and treated with DMSO, 125μM OI or 250μM OI, respectively, for 16 hours in a cell culture incubator. 10 dishes of cells were treated (4 dishes with DMSO, 3 dishes with 125μM OI and 3 dishes with 250μM OI) in each replicate experiment for utilizing TMT-10plex isobaric label reagent. Cells were harvested and washed with PBS twice. Each cell pellet was lysed on ice with 100μL of 0.5% CHAPS buffer containing 1x EDTA-free Pierce Halt protease inhibitor cocktail and 1x benzonase for 30min. Lysate was collected by centrifugation (20,000 g, 15 min) at 4°C to remove debris. Protein concentration was determined using a BCA protein assay kit. Lysates (0.4 mg from each dish, 4mg/ml) were then incubated with 500 μM of IA-DTB for 1 hour, followed by 5 mM DTT for 30 min, and 20 mM iodoacetamide for 30 min at room temperature in the dark. The resulting lysate was precipitated by 400 μL methanol, 100 μL chloroform, and 300 μL water. The precipitated protein was centrifuged at 4000 g for 10 min at 4°C, washed twice with 500 μL methanol with sonicating briefly each time to break up the protein pellet. Washed protein pellet was resuspended in 200 μL of 0.2 M EPPS buffer (pH 8.5) with brief sonication and digested with 8 μg of trypsin/Lys-C overnight at 37 °C shaking at 500 rpm. TMT-10plex reagents (0.8 mg in each reagent) were resuspended in dry acetonitrile, added to the digested samples, and incubated for 1 hr in a thermomixer at room temperature with shaking at 500 rpm. Afterwards, the TMT labeling reaction was terminated by adding 50% hydroxylamine (0.3% final concentration) to the mixture and incubate for 15 min. The labeled peptide samples were dried in a speedvac. 600 μL of 50% streptavidin resin slurry was washed with 10ml PBS three times. Dried peptides were resuspended in 1 mL PBS and pooled together to incubate with the streptavidin resin overnight at 4 °C. Resin was washed three times each with PBS, followed by PBS containing 0.1% SDS, and water to remove non-specific binding peptides from the resin. Resin-bound peptides were eluted by incubating the resin with 500 μL of elution buffer (50% acetonitrile + 0.1% TFA) in a Thermomixer shaking at 1000 rpm for 10 min. Resin was centrifuged to collect supernatant. Repeat elution with 200 μL of elution buffer and combined supernatant was dried in speedvac. The dried peptide was resuspended in 300 μL 0.1% TFA and subjected to Pierce High pH Reversed-Phase Peptide Fractionation Kit following manufacturer's protocol.

Fractionated peptides were reconstituted in 20 μL 0.1% formic acid. Samples were then analyzed by LC-MS/MS on a Fusion Lumos mass spectrometry. Around 0.5 μg of total peptides from each fraction were analyzed on an UltiMate 3000 nano-LC system (Thermo) coupled via a 25-cm C18 column (EASY-Spray, Thermo). Peptides were separated at a flow rate of 250 nL min^{-1} with a linear 110 min gradient from 2% to 35% solvent B (100% acetonitrile, 0.1% formic acid). Each sample was run for 120 min, including sample loading and column equilibrating times. Data were acquired in data-dependent mode. MS1 spectra were measured with a resolution of 120,000, an automatic gain control target of 4e5, maximum injection time 50 ms, and a mass range from 300 to 1800 *m/z*. MS2 spectra were collected using top-speed mass spec method within 3s of cycle time at a resolution of 50,000, an automatic gain control target of 8e5, an isolation window of 1.0 *m/z* and a normalized collision energy of 38.

All raw data were analyzed with MaxQuant software version 1.6.15.0. Spectral searches were performed using 10plex TMT as the isobaric labels. Carbamidomethylation of cysteine residues was set as fixed modification, while oxidation of methionine residues, acetylation of protein N-term and IA-DTB on cysteine residues were set as variable modifications. Competition ratio was calculated by dividing the TMT reporter ion intensities from control channel (DMSO) by the OI treated channel.

JAK1 structural modeling

The model of the JH1-JH2 domains of JAK1 was created by superimposing coordinates for the JAK1 JH1 (PDB: 5WO4) (Siu et al., 2017) and JH2 (PDB: 4L00) (Toms et al., 2013) domains onto a previously solved JAK family JH1-JH2 structure (PDB: 4OLI) (Lupardus et al., 2014). The overall complex was created and minimized in the program MAESTRO (Schrödinger Release 2021-2: Maestro, Schrödinger, LLC, New York, NY, 2021). 4 cysteine residues were highlighted in spheres. The model of itaconate covalently bound to Cys817 was created using CovDock in Schrödinger Release 2021-2 (Zhu et al., 2014).

QUANTIFICATION AND STATISTICAL ANALYSIS

Statistical analyses were carried out using GraphPad Prism 9 (GraphPad) software. A Student's t test was used to compare two groups affected by a single variable, whereas a one-way ANOVA followed by Sidak's multiple comparisons test was used to compare multiple groups. Details of the n number (representing biological replicates) can be found in the appropriate figure legend. Data are displayed as mean ± SEM or as individual data points. Differences were considered statistically significant at P values of *$p \leq 0.05$. ** signifies a P value of ≤ 0.01, *** signifies a P value of ≤ 0.001, and **** signifies a P value of < 0.0001.

Cell Metabolism, Volume *34*

Supplemental information

Itaconate and itaconate derivatives target JAK1 to suppress alternative activation of macrophages

Marah C. Runtsch, Stefano Angiari, Alexander Hooftman, Ridhima Wadhwa, Yanling Zhang, Yunan Zheng, Joseph S. Spina, Melanie C. Ruzek, Maria A. Argiriadi, Anne F. McGettrick, Rui Santalla Mendez, Alessia Zotta, Christian G. Peace, Aoife Walsh, Roberta Chirillo, Emily Hams, Padraic G. Fallon, Ranjith Jayaraman, Kamal Dua, Alexandra C. Brown, Richard Y. Kim, Jay C. Horvat, Philip M. Hansbro, Chu Wang, and Luke A.J. O'Neill

Supplemental figure 1 (Related to Figure 1)

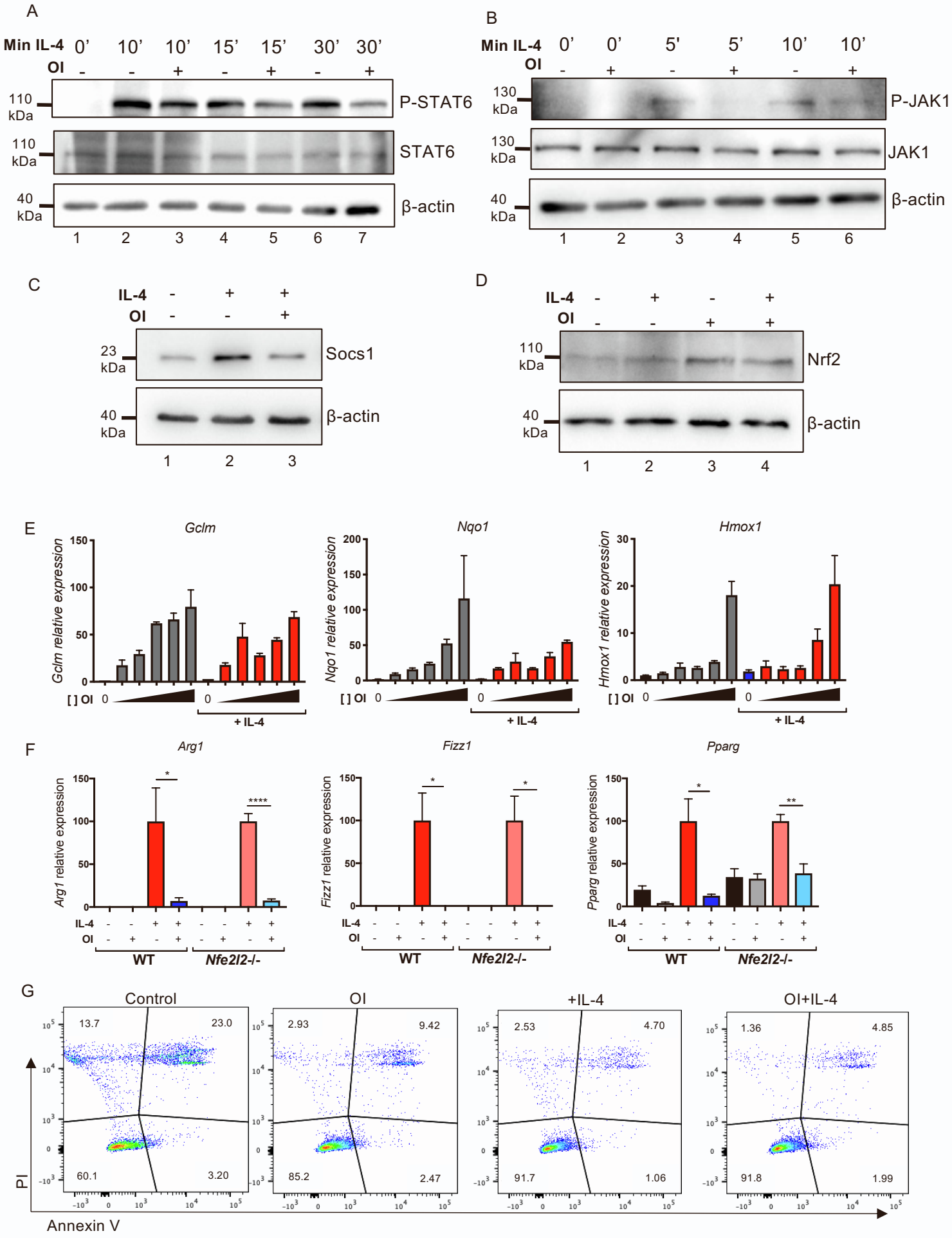

Supplemental Figure 1: OI inhibits the IL-4 JAK/STAT signaling pathway and activates NRF2 (Related to Figure 1)

(a) BMDMs were pretreated with OI or DMSO (control) for 2 hours, followed by stimulation with IL-4 for 10, 15, or 30 minutes. Western blot performed on cell lysates for phosphorylated STAT6 (P-STAT6), total STAT6, and β-actin housekeeping control. Showing one representative blot of n=3. **(b)** BMDMs were pretreated with OI or DMSO (control) for 2 hours, followed by stimulation with IL-4 for 0, 5, or 10 minutes. Western blot performed on cell lysates for phosphorylated JAK1 (P-JAK1), total JAK1, and β-actin housekeeping control. Showing one representative blot of n=3. **(c)** BMDMs were pretreated with OI for 2 hours, followed by stimulation with IL-4 for 1 hour. Western blot performed on cell lysates for Socs1 and β-actin housekeeping control. Showing one representative blot of n=3. **(d)** WT BMDMs were pretreated with OI for 2 hours, then stimulated with IL-4 for 24 hours. Western blot performed on cell lysates for Nrf2 and β-actin housekeeping control. Showing one representative blot of n=3. **(e)** BMDMs were pretreated with DMSO (vehicle control; 0μM OI) or increasing concentrations of OI for 2 hours, then stimulated with media or IL-4 for 24 hours. The triangle represents increasing OI concentrations ([ ] OI) starting from the left: 31.25 μM, 62.5 μM, 125 μM, 250 μM, and 500 μM. qRT-PCR results showing mRNA expression of NRF2-induced genes *Gclm*, *Nqo1*, and *Hmox1*, all normalized to *18s*. n=3. **(f)** WT or *Nfe2l2-/-* (NRF2-null) BMDMs were pretreated with OI for 2 hours, then stimulated with IL-4 or media alone for 24 hours. qRT-PCR results showing mRNA expression of *Arg1*, *Fizz1*, and *Pparg*, all normalized to *18s* and values adjusted to percent inhibition of IL-4 alone induced samples. n=4 for both WT and *Nfe2l2-/-*. **(g)** Representative flow plots from Figure 1o, showing annexin V surface expression and the DNA dye propidium iodide (PI).

Supplemental figure 2 (Related to Figure 1)

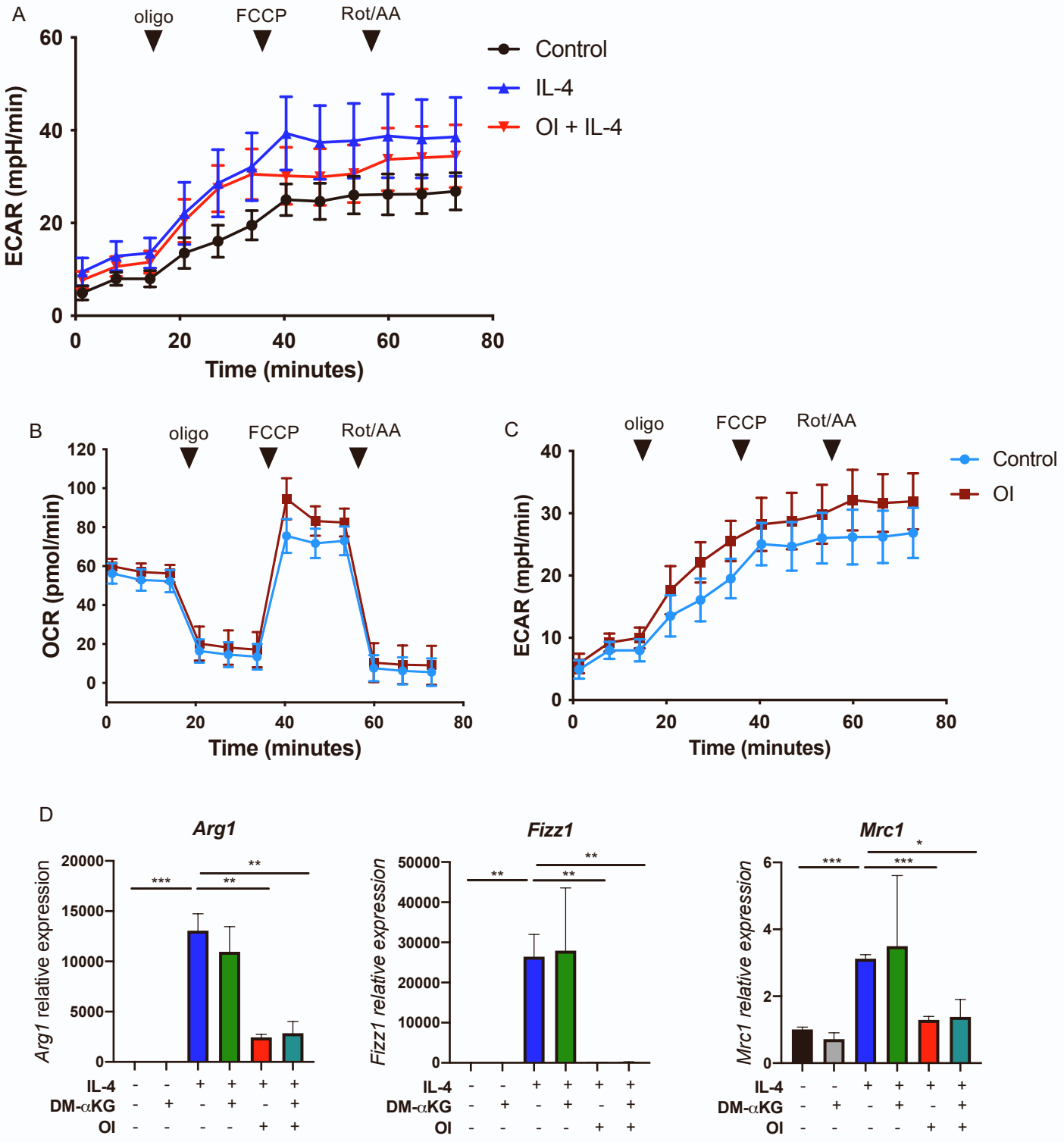

Supplemental figure 2: OI does not affect glycolysis, basal OXPHOS, and glutamine metabolism in M2 macrophages (Related to Figure 1)

(a) WT BMDMs were pretreated with OI for 2 hours, then stimulated with IL-4 for 24 hours. Seahorse data showing extracellular acidification rate (ECAR) of cells over time after addition of oligomycin (oligo), carbonyl cyanide-4-phenylhydrazone (FCCP), and rotenone/antimycin A (Rot/AA), in unstimulated cells (control), IL-4 alone, or OI + IL-4. n=6. **(b)** Seahorse data showing oxygen consumption rate (OCR) over time after addition of oligomycin (oligo), carbonyl cyanide-4-phenylhydrazone (FCCP), and rotenone/antimycin A (Rot/AA), in unstimulated BMDMs with or without OI treatment, after 26 hours. n=6. **(c)** Seahorse data showing ECAR over time after addition of oligomycin (oligo), carbonyl cyanide-4-phenylhydrazone (FCCP), and rotenone/antimycin A (Rot/AA), in unstimulated BMDMs with or without OI treatment, n=6. **(d)** WT BMDMs were pretreated with media, dimethyl alpha-ketoglutarate (DM-αKG), and/or OI for 2 hours, followed by IL-4 stimulation for 24 hours. qRT-PCR results showing mRNA expression of *Arg1*, *Fizz1*, and *Mrc1*, all normalized to *18s.* n=3.

Supplemental Figure 3 (Related to Figure 3)

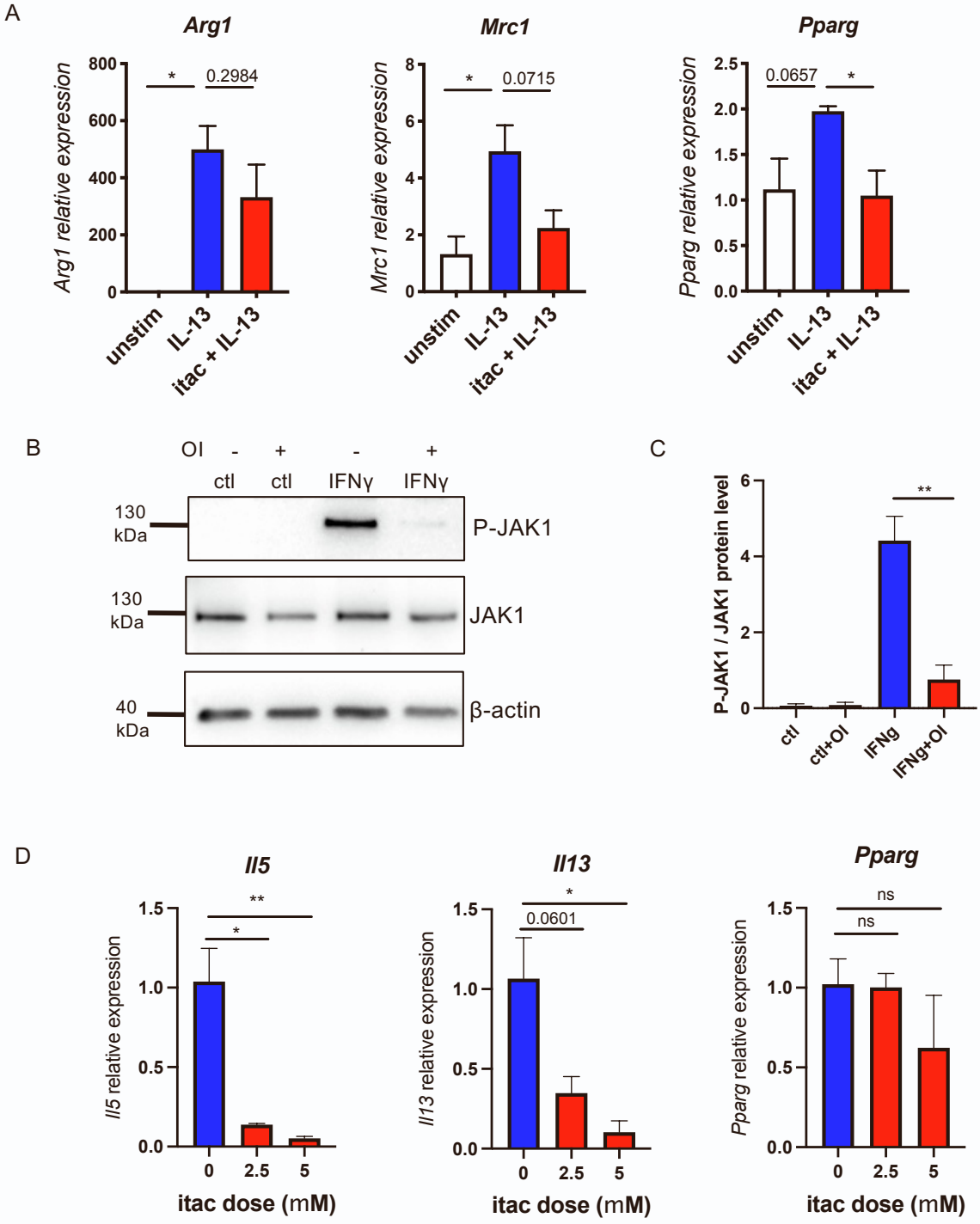

Supplemental Figure 3: Itaconate inhibits IL-13-induced and Th2 genes (Related to Figure 3)

(a) WT BMDMs were pretreated with 5mM itaconate for 2 hours, then stimulated with IL-13 for 24 hours. qRT-PCR results showing mRNA expression of *Arg, Mrc1, and Pparg,* normalized to *18s*. n=3. **(b)** WT BMDMs were pretreated with 5mM itaconate for 2 hours, then stimulated with IFNγ for 0.5 hours. Western blot performed on cell lysates for phosphorylated JAK1 (Tyr1034/1035), total JAK1, and β-actin housekeeping control. Showing one representative blot of n=6. **(c)** Western blot densitometry values of phosphorylated JAK1 (Tyr1034/1035) normalized to total JAK1 protein in BMDMs treated with the indicated label. n=3. **(d)** Murine splenic naïve $CD4^+$ T cells were treated with 0 mM, 2.5 mM, or 5 mM itaconate (pH 7.4), activated with αCD3/CD28 and skewed to Th2 with IL-4 and α-IFNγ for 72 hours. qRT-PCR results showing mRNA expression of *Il5*, *Il13*, and *Pparg*, all normalized to *Tbp*. n=3, 2 experimental repeats.

Supplemental Figure 4 (Related to Figure 4)

A

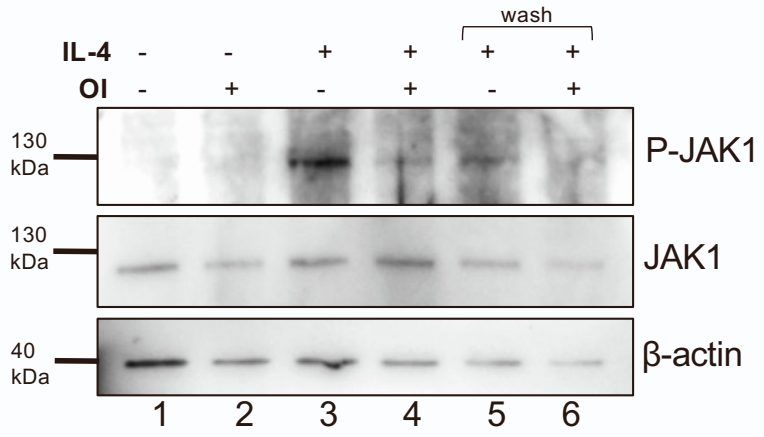

B

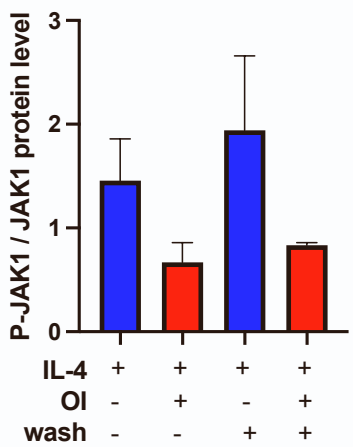

C

JAK1 ITalk Spectra

Replicate	Protein	Sites	Modified Peptides	Spectral Counts
1	sp|P52332|JAK1_MOUSE	715	K.QLASALSYLEDKDLVHGNVC*TK.N	3
	sp|P52332|JAK1_MOUSE	816	R.CRPVTPSC*KELADLMTR.C	2
	sp|P52332|JAK1_MOUSE	1130	R.KC*WEFQPSNR.T	2
	sp|P52332|JAK1_MOUSE	943	K.YKGIC*MEDGGNGIK.L	1
2	sp|P52332|JAK1_MOUSE	715	K.QLASALSYLEDKDLVHGNVC*TK.N	3
	sp|P52332|JAK1_MOUSE	816	R.CRPVTPSC*K.E	3
	sp|P52332|JAK1_MOUSE	1130	R.KC*WEFQPSNR.T	2
	sp|P52332|JAK1_MOUSE	943	K.YKGIC*MEDGGNGIK.L	2
3	sp|P52332|JAK1_MOUSE	715	K.QLASALSYLEDKDLVHGNVC*TK.N	3
	sp|P52332|JAK1_MOUSE	816	R.CRPVTPSC*KELADLMTR.C	2
	sp|P52332|JAK1_MOUSE	1130	R.KC*WEFQPSNR.T	2
	sp|P52332|JAK1_MOUSE	943	K.GIC*MEDGGNGIK.L	2

D

Proteins Modified by OI in Primary Human Macrophages

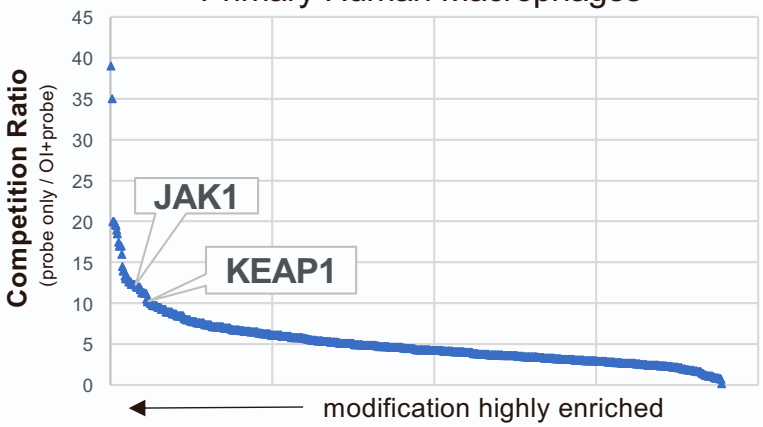

E

Alignment of Rat, Mouse, and Human JAK1 pseudokinase and kinase domain

```
TR|G3V9W2|G3V9W2_RAT VRDVENIMVEEFVEGGPLDLFMHRKSDALTTPWKFKVAKQLASALSYLEDKDLVHGNVCT 716
SP|P23458|JAK1_HUMAN VRDVENIMVEEFVEGGPLDLFMHRKSDVLTTPWKFKVAKQLASALSYLEDKDLVHGNVCT 717
SP|P52332|JAK1_MOUSE VRDVENIMVEEFVEGGPLDLFMHRKSDALTTPWKFKVAKQLASALSYLEDKDLVHGNVCT 716
                     ****************************.********************************

TR|G3V9W2|G3V9W2_RAT KNLLLAREGIDSDIGPFIKLSDPGIPVSVLTRQECIERIPWIAPECVEDSKNLSVAADKW 776
SP|P23458|JAK1_HUMAN KNLLLAREGIDSECGPFIKLSDPGIPITVLSRQECIERIPWIAPECVEDSKNLSVAADKW 777
SP|P52332|JAK1_MOUSE KNLLLAREGIDSDIGPFIKLSDPGIPVSVLTRQECIERIPWIAPECVEDSKNLSVAADKW 776
                     ************: ************::**:******************************

TR|G3V9W2|G3V9W2_RAT SFGTTLWEICYNGEIPLKDKTLIEKERFYESRCRPVTPSCKELADLMTRCMNYDPNQRPF 836
SP|P23458|JAK1_HUMAN SFGTTLWEICYNGEIPLKDKTLIEKERFYESRCRPVTPSCKELADLMTRCMNYDPNQRPF 837
SP|P52332|JAK1_MOUSE SFGTTLWEICYNGEIPLKDKTLIEKERFYESRCRPVTPSCKELADLMTRCMNYDPNQRPF 836
                     ************************************************************

TR|G3V9W2|G3V9W2_RAT FRAIMRDINKLEEQNPDIVSEKQPITEVDPTHFEKRFLKRIRDLGEGHFGKVELCRYDPE 896
SP|P23458|JAK1_HUMAN FRAIMRDINKLEEQNPDIVSEKKPATEVDPTHFEKRFLKRIRDLGEGHFGKVELCRYDPE 897
SP|P52332|JAK1_MOUSE FRAIMRDINKLEEQNPDIVSEKQPTTEVDPTHFEKRFLKRIRDLGEGHFGKVELCRYDPE 896
                     ********************:* ************************************

TR|G3V9W2|G3V9W2_RAT GDNTGEQVAVKSLKPESGGNHIADLKKEIEILRNLYHENIVKYKGICMEDGGNGIKLIME 956
SP|P23458|JAK1_HUMAN GDNTGEQVAVKSLKPESGGNHIADLKKEIEILRNLYHENIVKYKGICTEDGGNGIKLIME 957
SP|P52332|JAK1_MOUSE GDNTGEQVAVKSLKPESGGNHIADLKKEIEILRNLYHENIVKYKGICMEDGGNGIKLIME 956
                     ************************************************ ************

TR|G3V9W2|G3V9W2_RAT FLPSGSLKEYLPKNKNKINLKQQLKYAIQICKGMDYLGSRQYVHRDLAARNVLVESEHQV 1016
SP|P23458|JAK1_HUMAN FLPSGSLKEYLPKNKNKINLKQQLKYAVQICKGMDYLGSRQYVHRDLAARNVLVESEHQV 1017
SP|P52332|JAK1_MOUSE FLPSGSLKEYLPKNKNKINLKQQLKYAIQICKGMDYLGSRQYVHRDLAARNVLVESEHQV 1016
                     ****************************:********************************

TR|G3V9W2|G3V9W2_RAT KIGDFGLTKAIETDKEYYTVKDDRDSPVFWYAPECLIQCKFYIASDVWSFGVTLHELLTY 1076
SP|P23458|JAK1_HUMAN KIGDFGLTKAIETDKEYYTVKDDRDSPVFWYAPECLMQSKFYIASDVWSFGVTLHELLTY 1077
SP|P52332|JAK1_MOUSE KIGDFGLTKAIETDKEYYTVKDDRDSPVFWYAPECLIQCKFYIASDVWSFGVTLHELLTY 1076
                     ************************************:*.**********************

TR|G3V9W2|G3V9W2_RAT CDSDFSPMALFLKMIGPTHGQMTVTRLVNTLKEGKRLSCPPNCPDEVYQLMRKCWEFQPS 1136
SP|P23458|JAK1_HUMAN CDSDSSPMALFLKMIGPTHGQMTVTRLVNTLKEGKRLPCPPNCPDEVYQLMRKCWEFQPS 1137
SP|P52332|JAK1_MOUSE CDSDFSPMALFLKMIGPTHGQMTVTRLVKTLKEGKRLPCPPNCPDEVYQLMRKCWEFQPS 1136
                     **** ************************:******** **********************

TR|G3V9W2|G3V9W2_RAT NRTTFQNLIEGFEALLK 1153
SP|P23458|JAK1_HUMAN NRTSFQNLIEGFEALLK 1154
SP|P52332|JAK1_MOUSE NRTTFQNLIEGFEALLK 1153
                     ***:*************
```

Supplemental Figure 4: OI covalently modifies JAK1 (Related to Figure 4)
(a) WT BMDMs were pretreated with OI for 2 hours, then stimulated with IL-4 for 1 hour. In the last two lanes (5 and 6) labeled "wash", OI-treated media was removed, cells were washed with PBS, and then fresh media was added before IL-4 stimulation. Showing one representative blot of n=3. **(b)** Western blot densitometry values of phosphorylated JAK1 normalized to total JAK1 protein in BMDMs treated with the indicated label. n=3. **(c)** HEK293T cells were transfected with a rat JAK1-FLAG overexpression plasmid for 24h before cells were lysed. Lysates were then treated with 1 mM ITalk for 2 hours, and JAK1 was purified for mass spec analysis. LC-MS/MS spectra values of JAK1 modification on C715, C816, C1130, C943 by ITalk, showing cysteine modifications observed in 3 independent experimental repeats. **(d)** $CD14^+$ monocytes were sorted from PBMCs from human donors, differentiated into macrophages with MCSF, then treated with 125 μM OI or DSMO, followed by 150 μM ITalk, and lysates were collected. Mass spectrometry was performed to identify all proteins modified by OI significantly over ITalk probe alone. Plot shows individual human proteins (blue triangles) sorted by competition ratio, with a higher competition ratio denoting greater enrichment in 2,3-dicarboxypropylation of that protein by OI. JAK1 and KEAP1 are highlighted as top hits in this screen modified by OI. **(e)** Uniprot amino acid sequence alignment of rat, human, and mouse JAK1 pseudokinase and kinase domains, showing conservation of the three species. The cysteine residues highlighted in green indicate the sites modified by ITalk, while C816/817 highlighted in yellow, was modified by both ITalk and OI.